# Assessing the ability to quantify the decrease of $NO_x$ anthropogenic emissions in 2019 compared to 2005 using OMI and TROPOMI satellite observations

Audrey Fortems-Cheiney[1,*], Gregoire Broquet[1], Elise Potier[1,*], Antoine Berchet[1], Isabelle Pison[1], Adrien Martinez[1], Robin Plauchu[1], Rimal Abeed[1], Aurélien Sicsik-Paré[1], Gaelle Dufour[2], Adriana Coman[3], Dilek Savas[2], Guillaume Siour[3], Henk Eskes[4], Hugo Denier van der Gon[5], and Stijn Dellaert[5]

[1]Laboratoire des Sciences du Climat et de l'Environnement, CEA-CNRS-UVSQ, Gif-sur-Yvette, France
[2]Université Paris Cité and Univ Paris Est Créteil, CNRS, LISA, F-75013 Paris, France
[3]Univ Paris Est Créteil and Université Paris Cité, CNRS, LISA, F-94010 Créteil, France
[4]Royal Netherlands Meteorological Institute (KNMI), De Bilt, the Netherlands
[5]Department Air Quality and Emissions Research, TNO, P.O. Box 80015, 3508 TA Utrecht, Netherlands
[*]now in Science Partners, Quai de Jemmapes, 75010 Paris, France

**Correspondence to:** Audrey Fortems-Cheiney (audrey.fortems@science-partners.com)

**Abstract.** There are great expectations about the detection and the quantification of $NO_x$ emissions using $NO_2$ tropospheric columns from satellite observations and inverse systems. This study assesses the potential of the OMI-QA4ECV and TROPOMI satellite observations to improve the knowledge on European $NO_x$ emissions at the regional scale and to inform about the spatio-temporal variability of $NO_x$ anthropogenic emissions **in 2019 compared to 2005**, at the resolution of 0.5° over Europe. We first characterize the level of consistency between retrievals from OMI-QA4ECV and from the more recent reprocessing of the TROPOMI data, called TROPOMI-RPRO-v02.04, and the implications of the possible inconsistencies for inversions. Furthermore, starting from European emission estimates from the TNO-GHGco-v3 inventory for the year 2005, regional inversions using the Community Inversion Framework coupled to the CHIMERE chemistry-transport model and assimilating satellite $NO_2$ tropospheric columns from OMI and TROPOMI have been performed to estimate the European annual and seasonal budgets for the year 2019. Both the OMI and TROPOMI inversions show decreases in European $NO_x$ anthropogenic emission budgets **in 2019 compared to 2005**. Nevertheless, the magnitude of the reductions of the $NO_x$ anthropogenic emissions are different with OMI and TROPOMI data, with decreases in EU-27+UK between 2005 and 2019 of 16% and 45%, respectively. A TROPOMI inversion giving more weight to the satellite data becomes consistent with the independent TNO-GHGco-v3 inventory for the year 2019, with annual budgets for EU-27+UK showing absolute relative difference of only 4%. These TROPOMI inversions are therefore in agreement with the magnitude of the decline in $NO_x$ emissions declared by countries, when aggregated at the European scale. However, our results —with OMI and TROPOMI data leading to different magnitudes of corrections on $NO_x$ anthropogenic emissions—suggest that more observational constraints would be required to sharpen the European emission estimates.

## 1 Introduction

Air pollution is still a major health concern in Europe (EEA, 2023). Particularly, up to now all European Union (EU) countries report levels of nitrogen dioxide ($NO_2$) above the 2021 World Health Organization (WHO) global air quality guidelines, and around 64,000 premature deaths are caused by $NO_2$ pollution each year (EEA, 2023). In Europe, the main sources of $NO_2$ are road transport —responsible for 39% of the emissions in 2019 (EEA, 2022), thermal power plants and industrial activities (EEA, 2023). $NO_2$ is mainly produced in the atmosphere by the oxidation of nitric oxide (NO), which is emitted by the same activities.

To reduce $NO_2$ concentrations to levels that do not impact human health, nitrogen oxides ($NO_x$=NO+$NO_2$) emissions need to be cut down. The EU has comprehensive regulations governing air quality. The key legal instrument in this regard is the Ambient Air Quality Directive (2008/50/EC). In addition, there are other EU regulations and directives that address specific aspects of air quality, such as the National Emission Ceilings (NEC) Directive (2016/2284/EU) (OJE, 2016), which sets expected reductions of $NO_x$ emissions compared with 2005, often considered as the baseline year of regulation policies. To design efficient regulatory policies and assess their effectiveness, an accurate account of emissions in space and time is essential.

Budgets and sectoral distributions for air pollutants often come from bottom-up (BU) inventories, based on the statistics of socio-economic activities and fuel consumption and on emission factors per activity type. According to these BU inventories, $NO_x$ anthropogenic emissions have been strongly decreased –by about 36%– in Europe since 2005 (EEA, 2021). However, the quantification of anthropogenic $NO_x$ emissions following a BU approach suffers from relatively large uncertainties, especially from those in the emission factors, for which average values are generally used despite the large spatial and temporal variability of the actual factors. For instance, the European Monitoring and Evaluation Programme (EMEP) inventory reports 50-200% uncertainties in their sectoral budgets of $NO_x$ anthropogenic emissions at the national and annual scales (Kuenen and Dore, 2019). According to Schindlbacher et al. (2021), the uncertainty estimates for national anthropogenic $NO_x$ emissions range from 5% to 56% in Europe. The spatial distribution and temporal variability of the timeseries of emission inventory maps often rely on simple proxies and typical temporal profiles, which inevitably introduce errors. Quantifying natural (biogenic) emissions is also a complex issue (Guenther et al., 2006).

Since the year 2000, observations of the atmospheric concentrations of nitrogen dioxide ($NO_2$) are retrieved from space-borne spectrometers with suitable measurement spectral bands, such as the Global Ozone Monitoring Experiment (GOME) (Burrows et al., 1999), GOME-2 (Munro et al., 2016), the SCanning Imaging Absorption spectroMeter for Atmospheric CHartographY (SCIAMACHY) (Burrows et al., 1995; Bovensmann et al., 1999), and the Ozone Monitoring Instrument (OMI) (Levelt et al., 2006, 2018). These instruments offer a daily global coverage with horizontal resolutions of several hundreds of $km^2$. The satellite observations provide information on the chemical composition of the atmosphere, and for the analysis of the variations of the $NO_2$ concentrations associated to economic changes or pollution control legislations over the last decades (van der A et al., 2008; Castellanos and Boersma, 2012; Schneider

et al., 2015; Lamsal et al., 2015; Krotkov et al., 2016; Miyazaki et al., 2017; Li and Wang, 2019; Georgoulias et al., 2019; Silvern et al., 2019; Fortems-Cheiney et al., 2021a; van der A et al., 2024).

In parallel, progress has been made to develop atmospheric transport and chemistry inverse modelling for the estimation of $NO_x$ anthropogenic and/or biogenic emissions based on the satellite observations of the $NO_2$ tropospheric vertical column densities (TVCDs), also referred to as top-down (TD) or inverse modelling. Such systems generally rely on the comparison between observed TVCDs and $NO_2$ simulations based on atmospheric chemistry transport models and on emission estimates from BU gridded inventories and land-surface models, to retrieve optimal emission estimates. The retrieval of these emission estimates assumes the discrepancies between simulated and observed TVCDs to be mainly due to these BU emission estimates.

However, the discrepancies between simulated and observed TVCDs are also due to errors in the modelling of the atmospheric transport and chemistry of $NO_x$ (Stavrakou et al., 2013) and in the observations due to instrumental errors and retrieval biases (Lorente et al., 2017). The retrieval of TVCDs with the corresponding averaging kernels relies on the local inverse modelling of the radiative transfer in the atmosphere under various and often complex atmospheric and surface conditions, which is challenging (Boersma et al., 2004; van Geffen et al., 2022a). Therefore, the intercomparisons of the different $NO_2$ retrieval products based on measurements from a specific satellite instrument but different algorithms reveal large differences. For instance, the magnitude of the OMI $NO_2$ TVCDs of OMI-NASAv3 (from the National Aeronautics and Space Administration; NASA) and of OMI-DOMINOv2 (from the Royal Netherlands Meteorological Institute; KNMI) differ by 50% over densely populated areas in China, and they show different trends over the past decade at the regional scale (Zheng et al., 2014; Qu et al., 2017; Lorente et al., 2017). Qu et al. (2020) compared OMI-NASAv3, OMI-DOMINOv2 and the Quality Assurance for Essential Climate Variables (OMI-QA4ECV) OMI $NO_2$ TVCD product, and showed that the different vertical sensitivities in the $NO_2$ retrievals explain for a large part the discrepancies between the retrieved $NO_2$ TVCDs.

The first $NO_x$ atmospheric inversions using satellite $NO_2$ data were generally based on global systems and targeted the variability of the $NO_x$ emissions at continental scales (Martin et al., 2003; Boersma et al., 2008; Stavrakou et al., 2008; Lamsal et al., 2011; Miyazaki et al., 2017). The scientific and societal needs for the quantification and mapping of pollutant emissions at a relatively high-spatial resolution fostered the use of regional-scale inversion systems, based on mesoscale chemistry transport models (CTM) and the analysis of the $NO_2$ concentrations at spatial resolution close to that of the satellite observations (Mijling and van der A, 2012; Mijling et al., 2013; Lin, 2012; Ding et al., 2017; Visser et al., 2019; Fortems-Cheiney et al., 2021b; Savas et al., 2023; van der A et al., 2024), and even down to a resolution of 10 km$\times$10 km (Plauchu et al., 2024).

The computation cost of the regional atmospheric inversions can be potentially high, due to the need to rely on high spatial resolution CTMs, and to manage high dimension inversion problems for the estimation of $NO_x$ emissions at relatively fine spatio-temporal scales that support the derivation of robust monthly to annual, national to sub-national budgets. To mitigate this computational cost, mass balance approaches have been employed (Visser et al., 2019). These approaches account for the non-linear relationships between $NO_x$ emission changes and $NO_2$ TVCDs via reactions with

hydroxyl radicals (OH) but with simple scaling factors. (Stavrakou et al., 2013; Ding et al., 2017; van der A et al., 2024) tend to indicate that a more robust account for the complex $NO_x$ chemistry is required for the accurate derivation of $NO_x$ emissions from $NO_2$ satellite data. In addition, with such an approach the emissions are scaled so that the CTM simulations perfectly fit to the observations, so that the errors from both the CTM and the retrievals are ignored, which can limit the accuracy of the inversions (Miyazaki et al., 2017). In this context, the complex Bayesian approaches with ensemble Kalman filter or variational inverse modeling techniques relying on CTMs may have a key role to play, since they are designed to take into account both i) the non-linearities of the $NO_x$ chemistry and ii) the errors from the CTMs and retrievals.

Since 2017, the TROPOspheric Monitoring Instrument (TROPOMI,Veefkind et al. (2012)) onboard the Copernicus Sentinel-5 Precursor (S5P) has been providing $NO_2$ TVCDs images (over a wide swath), at higher spatial resolutions and improved signal-to-noise ratio, compared to previous missions such as OMI (van Geffen et al., 2020). With variational inversions, Plauchu et al. (2024) assessed the potential of the TROPOMI observations to inform about $NO_x$ emissions in France from 2019 to 2021 at the national to urban scales. Their results open positive perspectives regarding the ability of inversions to support the validation or improvement of inventories with TROPOMI observations, at least at the local level for emission hotspots generating a relatively strong local signal, which are better caught and exploited by the inversions than the larger scale signals (Plauchu et al., 2024). While previous satellite instruments could already provide information over emission hot spots (e.g, over large urbans areas in Europe; (Fortems-Cheiney et al., 2021a)), TROPOMI might be now more relevant than these previous satellite instruments to monitor the $NO_x$ anthropogenic emissions (Zheng et al., 2020; Li et al., 2023).

In this context, this study assesses the respective potential of the OMI and TROPOMI satellite observations to inform about the decrease of $NO_x$ anthropogenic emissions in 2019 compared to 2005 at the continental to national scales in Europe, based on a state-of-the-art regional variational inverse modeling system. The concept is to assess the level of decrease in the emission estimates for the year 2019 from the atmospheric inversions assimilating OMI or TROPOMI observations for this year, compared to the prior estimate that they correct to better fit the observations, and which corresponds to an inventory for the year 2005. Such a concept accounts for the absence of TROPOMI observations in 2005, but parallel tests (e.g. with OMI observations in 2005) are conducted to ensure that this decrease fairly reflects the level of decrease in emissions between 2005 and 2019 caught by the inversions.

In practice, we have performed 1-year inversions using an estimate of the $NO_x$ anthropogenic emissions from the TNO-GHGco-v3 inventory (Dellaert et al., 2021) for the reference year 2005 to define the prior estimate of the variational inversions. The evaluation of the emissions estimated from the inversions is based on comparisons to the $NO_x$ emission estimates from the TNO-GHGco-v3 inventory for the year 2019. We use a European scale variational inverse modeling system at 0.5° and 1-day resolution based on the coupling of the variational mode of the Community Inversion Framework (CIF) (Berchet et al., 2021) to a 0.5° resolution configuration of the regional CTM CHIMERE (Menut et al., 2013). Our inversion system combines both the advantages of i) solving large dimensional inversion problems, i.e. controlling emissions at relatively high temporal and spatial resolution and assimilating a large amount of observations,

**and of ii) simulating $NO_2$ concentrations and the sensitivities of $NO_2$ tropospheric columns to surface emissions at a relatively high spatial resolution with a chemistry scheme, based on CHIMERE and its adjoint code. Our inversion system is therefore well designed to estimate $NO_x$ emissions at the 0.5° and 1d-resolutions, taking into account the non-linearities of the $NO_x$ chemistry. The CIF-CHIMERE variational inversion configuration has already been used for the estimation of the emissions of $NO_x$ (Savas et al., 2023; Plauchu et al., 2024) but also of other species such as CO (Fortems-Cheiney et al., 2024) and $CO_2$ (McGrath et al., 2023).**

**As a preliminary analysis, we have also characterized the level of consistency between retrievals from OMI-QA4ECV and from the more recent reprocessing of the TROPOMI data, called TROPOMI-RPRO-v02.04, and the implication of the possible inconsistencies for inversions. The regional 0.5° resolution simulations of $NO_2$ TVCDs in Europe with CHIMERE are used to indirectly analyze this consistency via the respective differences between the two $NO_2$ TVCD products and CHIMERE. In the following, we first describe the CHIMERE configuration for Europe, the $NO_2$ satellite observations, and the variational inversion method in Section 2. Section 3 presents our results, including the comparison between the CHIMERE simulations, the OMI and TROPOMI $NO_2$ TVCDs and the posterior estimates of $NO_x$ European anthropogenic emissions.**

## 2 Data and Methods

**The principle of our traditional atmospheric inversion approach is to correct *a priori* estimates of the emission maps, also denoted "prior emissions", to reduce differences between atmospheric observations and their simulations with a CTM fed with the estimates of emission maps. It relies on a specific Bayesian inversion algorithm, on satellite observations of the atmospheric densities of $NO_2$, and on a regional CTM, as shown in Figure 1. We detail these different components of our inversion framework: the CIF-CHIMERE variational inversion system, the prior estimates of the $NO_x$ emissions in Europe for the year 2005, the configuration of the CHIMERE CTM and of its adjoint code for the simulation of $NO_2$ concentrations and of their sensitivity to the emissions estimates, and the OMI-QA4ECV and TROPOMI satellite observations for the year 2019. The process ensuring a suitable comparisons between the simulations and the satellite observations -the aggregation of the observations into super-observations and the application of the averaging kernels from the satellite retrievals to the vertical columns of the model simulations - are also explained. Finally, we provide details about our configuration for the inversion of $NO_x$ emissions over Europe.**

### 2.1 The CIF-CHIMERE inversion system

The Community Inversion Framework (CIF) is a modular inverse modeling platform which can drive various data assimilation schemes and various CTMs (Berchet et al., 2021). Here, the CIF drives the CHIMERE CTM (Menut et al., 2013; Mailler et al., 2017) and its adjoint code (Fortems-Cheiney et al., 2021b). The coupling between the CIF and CHIMERE and its adjoint code and their use for variational inversions takes advantage of the developments in the Bayesian variational atmospheric inversion system PYVAR-CHIMERE to account for reactive species (Fortems-Cheiney et al., 2021b).

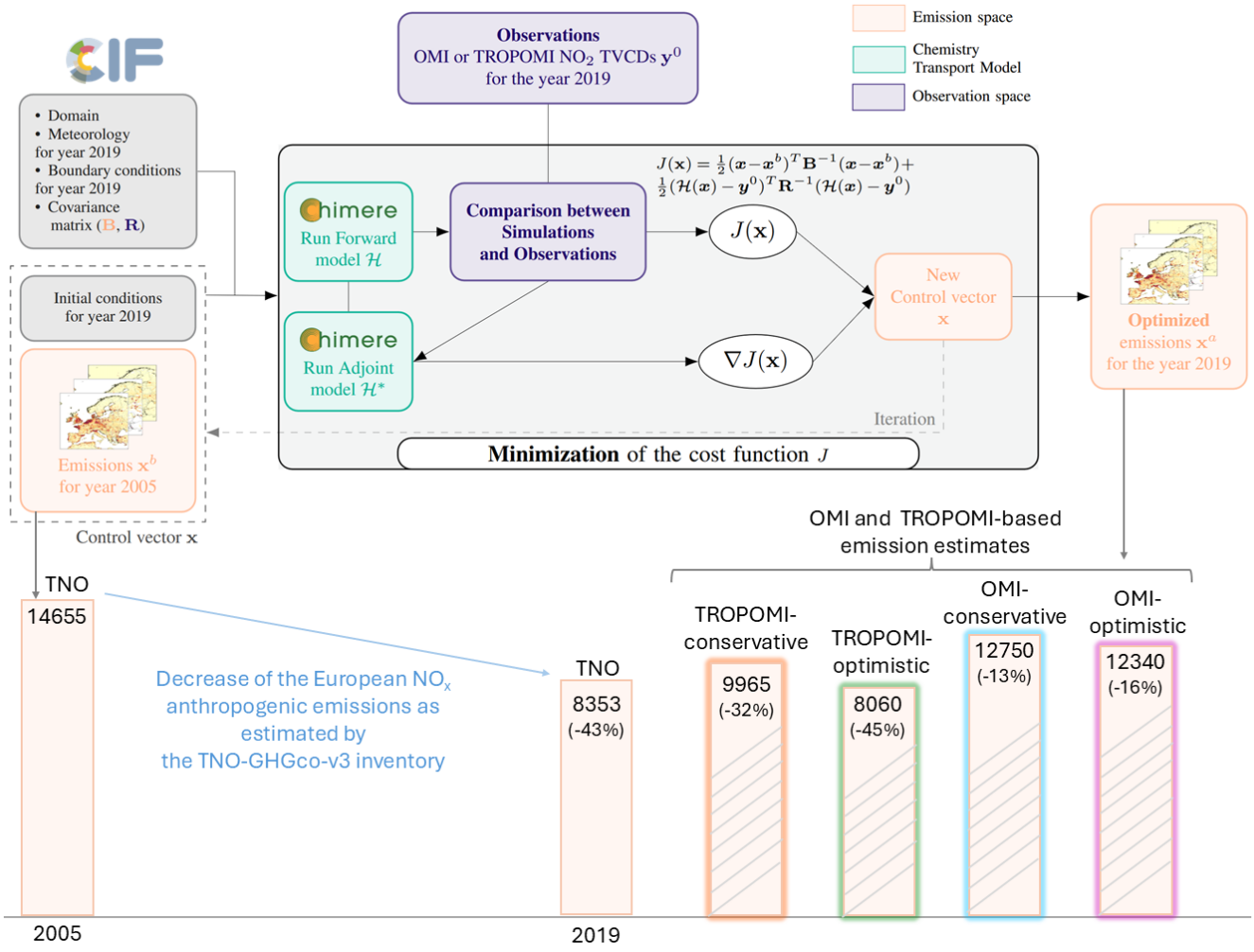


**Figure 1.** Simplified scheme of the iterative minimization in the CIF-CHIMERE inversion system and illustration of the decrease of the European $NO_x$ emissions estimated both by TNO and by the OMI and TROPOMI-based inversions. The different inversions are described in Table 1. The numbers express the anthropogenic $NO_x$ emission estimates for the EU-27+UK area in kteq$NO_2$. The numbers in brackets express the difference of the anthropogenic $NO_x$ emission estimates for the EU-27+UK in 2019 compared to 2005, in %.

### 2.2 Prior estimates of the $NO_x$ emissions in Europe

The prior estimates of $NO_x$ emissions in this study are based on anthropogenic $NO_x$ emission estimates from the TNO-GHGco-v3 gridded inventory (Dellaert et al., 2021) for the year 2005. We have chosen such an estimate for year 2005 to assess the potential of satellite observations for year 2019 to quantify the high spatio-temporal differences in the $NO_x$ emissions between
160 2005 and 2019. The $NO_x$ emission estimates from the TNO-GHGco-v3 inventory for the year 2019 is used to evaluate the inversion results. We have also performed inversions i) both using $NO_x$ prior emissions and assimilating satellite observations

for the year 2005 and ii) both using $NO_x$ prior emissions and assimilating satellite observations for the year 2019 (Table 1) to assess the impact of the prior inventory on the $NO_x$ emissions estimated from the inversions.

The TNO-GHGco version is an update of the TNO inventory documented in Kuenen et al. (2014) and in Super et al. (2020), based on country emission reporting to the European Monitoring and Evaluation Program (EMEP)/Center on Emission Inventories Projection (CEIP). The TNO-GHGco-v3 inventory maps $NO_x$ emissions at a $6\times6$ km$^2$ horizontal resolution. It combines emissions from area sources, set at the surface, and from point sources. Emissions from point sources, mainly from the energy production and the industrial sectors, are distributed on the first eight vertical model layers in CHIMERE depending on the typical injection heights provided in the TNO inventory, based on Bieser et al. (2011).

In the TNO inventory, annual and national budgets are disaggregated in space based on proxies of the different sectors (Kuenen et al., 2014). Temporal disaggregation is based on temporal profiles provided per GNFR sector code with typical month to month, weekday to week-end and diurnal variations (Ebel et al., 1994, Menut et al., 2011). Following the GENEMIS recommendations (Kurtenbach et al., 2001; Aumont et al., 2003), we have speciated the TNO-GHGco-v3 $NO_x$ emissions as 90% of NO, 9.2% of $NO_2$, and 0.8% of nitrous acid (HONO) emissions.

CHIMERE is fed with NO biogenic soil emissions from the Model of Emissions of Gases and Aerosols from Nature (MEGAN) model for the year 2019 (Guenther et al., 2006), with a ~$1\times1$ km$^2$ spatial resolution. MEGAN does not take the impact of agricultural practices into account, even though it covers both natural and agricultural areas. There are large uncertainties in the $NO_x$ emissions due to agriculture, and in principle, there could be some overlapping between the agricultural and purely natural soil $NO_x$ emission estimates. It explains why these emissions are not provided by the TNO inventory. Therefore, we do not include a specific agricultural soil $NO_x$ emissions component in our prior estimation of the $NO_x$ emissions. The lightning $NO_x$ fluxes, whose impact on $NO_2$ concentrations is very small in Europe even in summer (Menut et al., 2020), are not accounted for. Fire emissions are also ignored, as their contribution to the $NO_x$ total emissions and to the long-term $NO_2$ concentration trends over Europe is small. The anthropogenic emissions for volatile organic compounds (VOCs) are obtained from the EMEP inventory (Vestreng et al., 2005).

The different emission products have been aggregated at the $0.5°\times0.5°$ horizontal resolution of the CHIMERE grid. The maps of monthly budgets for total, anthropogenic and natural $NO_x$ emissions at 0.5° resolution are shown in Figure 2 for August 2019. Even in summer when the biogenic $NO_x$ emissions are high, the anthropogenic emissions contribute to about 95% of the total $NO_x$ emissions in Europe with a budget of about 815 kteq$NO_2$. This unit means that the mass of both NO and $NO_2$ emissions are calculated using the $NO_2$ molar mass.

### 2.3 Configuration of the CHIMERE CTM for the prior simulation of $NO_2$ concentrations in Europe

We present the configuration of the CHIMERE CTM used in this study and the specific elements of the simulation, which will be used as the prior of the variational inversions. Here, the configurations of CHIMERE and of its adjoint code are driven by the CIF to simulate $NO_2$ atmospheric concentrations over Europe over a $0.5°\times0.5°$ regular horizontal grid with 17 vertical layers, from the surface to 200 hPa, with 8 layers within the first two kilometres. The domain covers 15.25°W-35.75°E; 31.75°N-74.25°N and includes 101 (longitude) x 85 (latitude) x 17 (vertical levels) grid-cells.

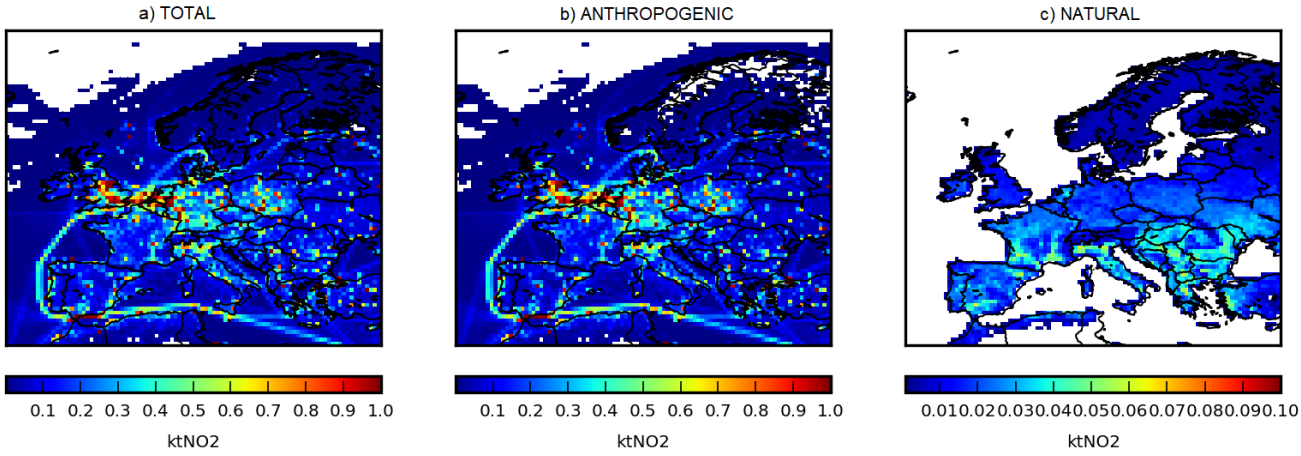


**Figure 2.** *Monthly budget of prior $NO_x$ emissions corresponding to the a) total, b) anthropogenic from the TNO-GHGco-v3 inventory and c) biogenic from the MEGAN model, per model grid-cell, in kteq$NO_2$, in August 2019. Note that the scale is different for anthropogenic and biogenic emissions.*

The chemical scheme used here is MELCHIOR-2, with more than 100 reactions, including 24 for inorganic chemistry (Lattuati, 1997; Derognat et al., 2003). **It accounts for non-linear relationships between $NO_x$ emission changes and $NO_2$ TVCDs via reactions with hydroxyl (OH) radicals but also with other direct or indirect $NO_x$ sinks associated with other species, such as ozone ($O_3$) or the $HO_2$ radical.** Due to the need for a compromise between the robustness of the simulation of the chemistry in the model and the computational cost with a complex chemical scheme, the aerosol modules of CHIMERE have not been included in its adjoint code yet and are therefore not activated in the CHIMERE forward simulations, as explained in Fortems-Cheiney et al. (2021b).

CHIMERE is driven here by the European Centre for Medium-Range Weather Forecasts (ECMWF) operational meteorological forecast for the year 2019 (Owens and Hewson, 2018). Considering $NO_2$ short lifetime, we do not consider its import from outside the domain. Nevertheless, the lateral and top boundaries for longer lived species such as ozone ($O_3$), nitric acid ($HNO_3$), peroxyacetyl nitrate (PAN), which participate to the $NO_x$ chemistry, are taken into account (Fortems-Cheiney et al., 2021b). Climatological values from the LMDZ-INCA global model (Szopa, 2008) are used to prescribe the concentrations of these species at the model boundaries.

### 2.4 Satellite Observations

**Among the instruments providing a long archive of $NO_2$ observations, OMI has the highest spatial resolution and least degradation through time (Levelt et al., 2018; Schenkeveld et al., 2017). OMI and TROPOMI present similarities: the retrievals from TROPOMI and from OMI-Q4ECV are based on similar algorithms, using the same prior profiles and assimilation technique to estimate the stratospheric column from the global model TM5-MP, and they make measure-**

**ments at nadir at about the same local time. Therefore, we expect these data sets to be consistent, with similar $NO_2$ TVCDs over horizontal and temporal scales larger than a few hundred kilometers resolution and the month. Nevertheless, a comparison of TROPOMI version 01.03 $NO_2$ TVCDs to OMI-QA4ECV observations shows differences in terms of monthly $NO_2$ average varying from a few % up to -40% over polluted regions (Western Europe, Eastern China, Eastern USA, Middle East), the largest differences occuring in winter (Lambert et al., 2021). Comparisons with ground-based measurements have also shown that versions v01.02 and v01.03 of TROPOMI data lead to $NO_2$ TVCDs that are too low by 22% to 37% for clean and slightly polluted scenes, and up to 51% over highly polluted areas (Verhoelst et al., 2021). Efforts have been made to correct such biases in the recent versions of the TROPOMI data, and seem to lead to a better agreement with OMI-QA4ECV observations and with ground-based measurements (Lambert et al., 2021; van Geffen et al., 2022b, a).**

As significant biases between the OMI and TROPOMI tropospheric columns have been described in previous studies in winter (Lambert et al., 2021; Verhoelst et al., 2021; van Geffen et al., 2022b), the month of January 2019 is being particularly used to compare these observations in the following.

### 2.4.1 OMI-QA4ECV-v1.1

The Ozone Monitoring Instrument (OMI) is an ultraviolet-visible (UV-Vis) instrument launched in July 2004 onboard the Earth Observation System (EOS) Aura satellite, which flies on a 705 km sun-synchronous orbit that crosses the Equator at approximately 13:40 LT. The nominal footprint of the OMI ground pixels is $24\times13$ km$^2$ (across$\times$along track) at nadir. With a swath of about 2600 km, it provided daily global coverage for $NO_2$ (no longer achieved due to the row anomaly). OMI uses the $O_2$-$O_2$ absorption feature for the cloud pressure retrieval (Veefkind et al., 2016).

The $NO_x$ inversions described in Section 2.5 assimilate $NO_2$ tropospheric vertical column densities (TVCDs) from the OMI-QA4ECV-v1.1 (www.qa4ecv.eu and http://temis.nl/qa4ecv/no2.html, Boersma et al., 2017, 2018). The data selection follows the criteria of the data quality statement (Boersma et al., 2017): the processing error flag equals 0, the solar zenith angle is lower than 80°, the snow ice flag is lower than 10 or equal to 255, the ratio of tropospheric air mass factor (AMF) over geometric AMF is higher than 0.2 to avoid situations in which the retrieval is based on very low (relative) tropospheric air mass factors and the cloud fraction is lower than 0.5. We use an additional criterion for the selection of the observation to be assimilated: the error associated to the retrieval must be lower than 100%. Note that the OMI-QA4ECV-v1.1 reprocessed data sets officially covers the period 2005-2018. This processing is using ERA-Interim 60 layer meteorological reanalyses from the ECMWF as driver. To facilitate comparisons with TROPOMI, the OMI dataset was further extended to 2019 using 137 layer ECMWF operational meteorological data. For 2019, the pressure levels are identical for the OMI and TROPOMI products.

### 2.4.2 TROPOMI RPRO-v02.04

The Tropospheric Monitoring Instrument (TROPOMI, (Veefkind et al., 2012)) was launched onboard the Copernicus Sentinel-5 Precursor (S5P) satellite in October 2017. It flies on a 824 km altitude sun-synchronous orbit that crosses the Equator at approximately 13:40 LT. This imaging spectrometer covers a UV-Vis band supporting the derivation of $NO_2$ TVCDs observa-

tions. The nominal footprint of the TROPOMI ground pixels is of about $7\times3.5$ km$^2$ before 6 August 2019 and $5.5\times3.5$ km$^2$ after 6 August 2019 at nadir. With a swath of about 2600 km on ground, it provides daily global coverage for $NO_2$. **Actually, one of the differences between the OMI and TROPOMI retrievals is the cloud pressure retrieval, which could have large impacts on the results. In particular, the Fast Retrieval Scheme for Clouds from Oxygen absorption band FRESCO-S version implemented for TROPOMI in v01.00 to v01.03 has been known to overestimate the cloud pressure, leading to a high bias in the air-mass factors and a low bias in the tropospheric columns (Lambert et al., 2021).** In addition, TROPOMI-v02.04 uses the TROPOMI dependent Lambertian-equivalent reflectivity (DLER) v1.0 surface albedo dataset (Tilstra et al., 2024), in contrast to OMI which makes use of the OMI Lambertian equivalent reflectance (LER) (Kleipool et al., 2008). Furthermore, TROPOMI applies dynamic albedo adjustments (van Geffen et al., 2022a) which is not done in the OMI-QA4ECV data set.

Our selection of the TROPOMI data to be assimilated in the inversions described in Section 2.5 follows the criteria of van Geffen et al. (2022b). We only select observations with a quality assurance (qa) value higher than 0.75. Like OMI, we only select observations when the error associated to the retrieval is lower than 100%.

### 2.4.3 Choices made to ensure a consistent comparison between simulated and observed $NO_2$ TVCDs

OMI and TROPOMI have different horizontal resolutions and more generally a different spatio-temporal sampling. The comparison between the data from the two instruments as well as the comparisons to the simulated TVCDs have therefore been done over a common projection, within the $0.5°\times0.5°$grid-cells of the CHIMERE CTM.

To make comparisons between simulations and satellite observations, the simulated vertical profiles are first interpolated on the satellite's levels, with a vertical interpolation from CHIMERE's levels. Then, the averaging kernels (AKs) from the OMI and TROPOMI products, respectively, are applied to the simulated profiles to account for the variations of the vertical sensitivity of the satellite retrievals (Eskes and Boersma, 2003; Boersma et al., 2017; van Geffen et al., 2022b). It is important to note that the OMI and the TROPOMI observations are accompanied with differences in their AKs, mainly explained by differences in their cloud pressure retrievals. The lower spatial resolution of OMI compared to TROPOMI also leads to differences in the distribution of the effective cloud fractions, with TROPOMI having relatively more cloud free and fully clouded pixels, which impacts the AKs and their shapes. Over land, OMI and TROPOMI present similar sensitivity near the surface, both over polluted areas defined as areas where the $NO_2$ TVCDs are higher than $2\times10^{15}$ molec.cm$^{-2}$ and over rural areas (Figure 3). However, due to lower cloud pressures on average in OMI than TROPOMI and consequently smaller air mass factors (AMFs) in the mid to lower troposphere, the AKs in OMI tend to be smaller than in TROPOMI above the first four levels of the satellites. These different vertical sensitivities and amplitudes of the AKs in the $NO_2$ OMI and TROPOMI retrievals will affect the simulated $NO_2$ TVCDs over Europe.

As the spatial resolution of OMI or TROPOMI data is finer than that of the chosen CTM model grid, the selected OMI or TROPOMI TVCDs are aggregated into "super-observations", as recommended by Rijsdijk et al. (2024). In order to associate the super-observations to an actual AK profile, the super-observations have been taken as the observation (TVCD and AKs) corresponding to the value closest to the mean of the OMI or TROPOMI TVCDs within the 0.5°×0.5° model grid-cell and

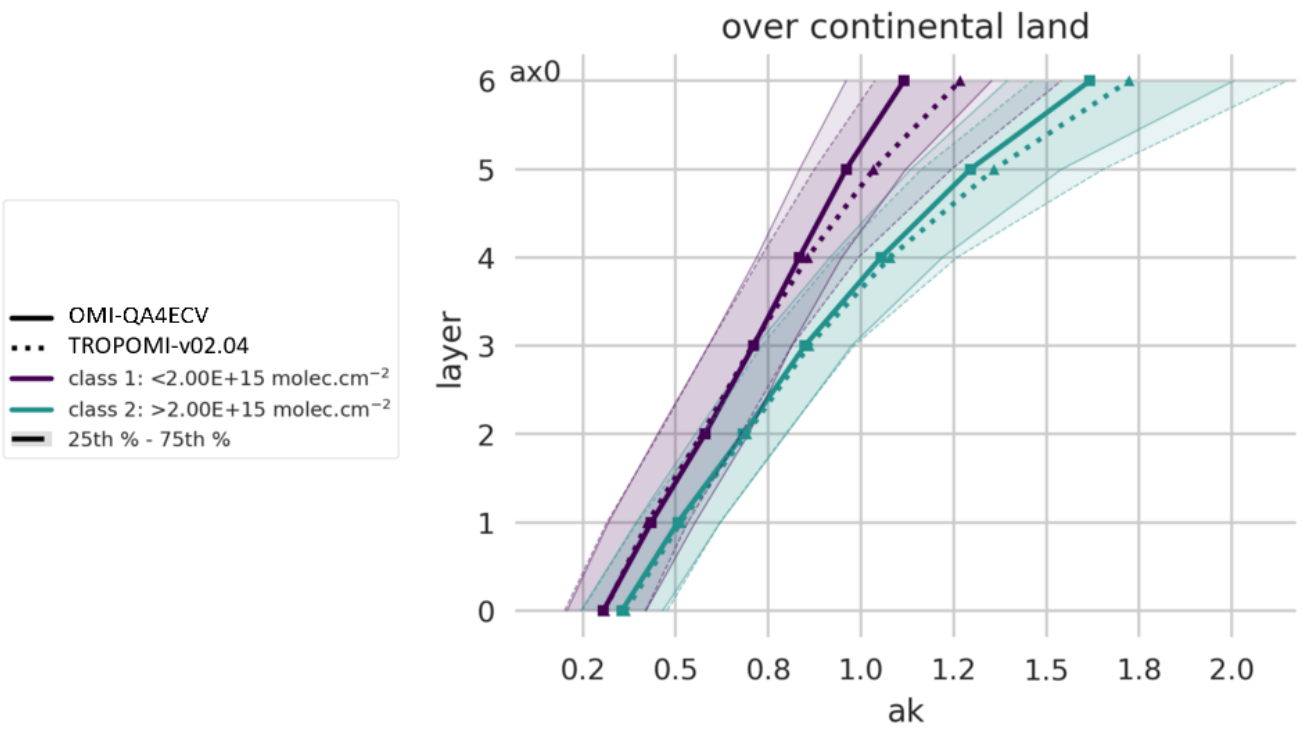


**Figure 3.** Median and quartile profiles of averaging kernels from OMI-QA4ECV and TROPOMI-RPRO-v02.04 super-observations over continental land, for $NO_2$ TVCDs lower and higher than $2\times10^{15}$ molec.cm$^{-2}$, for the first six levels of the satellites, in January 2019.

within the CHIMERE physical time step of about 5-10 minutes, as in Plauchu et al. (2024). The choice of the value closest to the mean is different from Fortems-Cheiney et al. (2021b), initially taking the median of the observations for defining super-observations. This choice was made necessary by the high number of TROPOMI observations within the $0.5°\times0.5°$ model grid-cell. The number of TROPOMI observations within a TROPOMI super-observation can reach 50, while the number of OMI observations within an OMI super-observation is often lower than five over continental land (Figure 4). We assume that over a set of a few tens of data the mean of the observations is more representative than the median, particularly in grid-cells with high concentrations. The number of TROPOMI and OMI super-observations is given as an example for the month of January 2019, respectively in Figure 5a and in Figure 5b. The TROPOMI super-observations present a coverage higher than the OMI ones by about a factor 4 (about 117,000 against 27,000). The only areas not really covered by TROPOMI are north-eastern Europe because of the snow cover and northern Europe because of the high solar zenith angle (Figure 5a).

The simulated $NO_2$ TVCDs corresponding to the OMI super-observations, using the OMI AKs, are called "CHIMERE-OMI". Similarly, the simulated $NO_2$ TVCDs corresponding to the TROPOMI super-observations, using the TROPOMI AKs, are called "CHIMERE-TROPOMI" in the following.

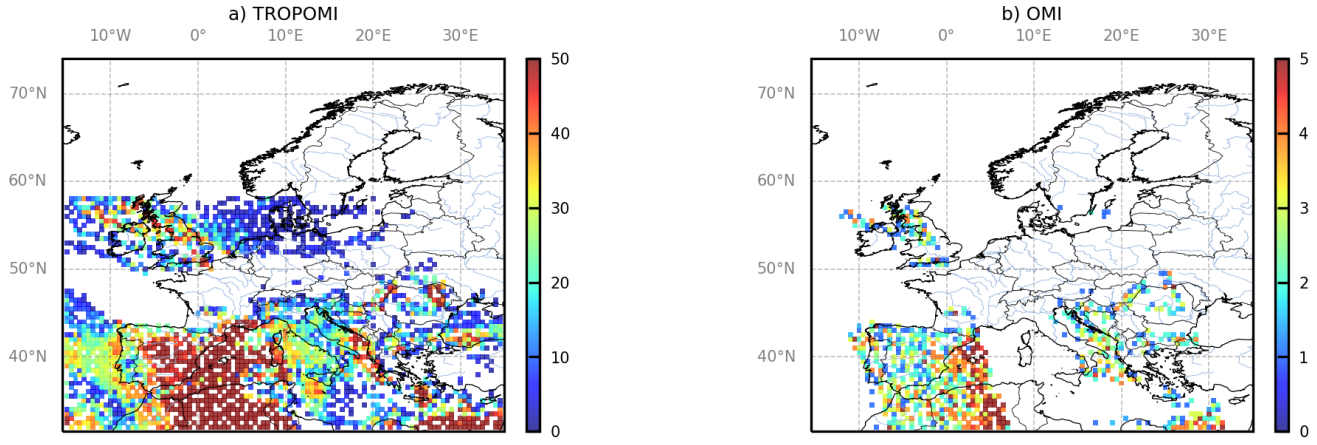


**Figure 4.** Daily number of observations within a) TROPOMI and b) OMI super-observations, for January the 1st in 2019. Note that the scales are different for TROPOMI and OMI.

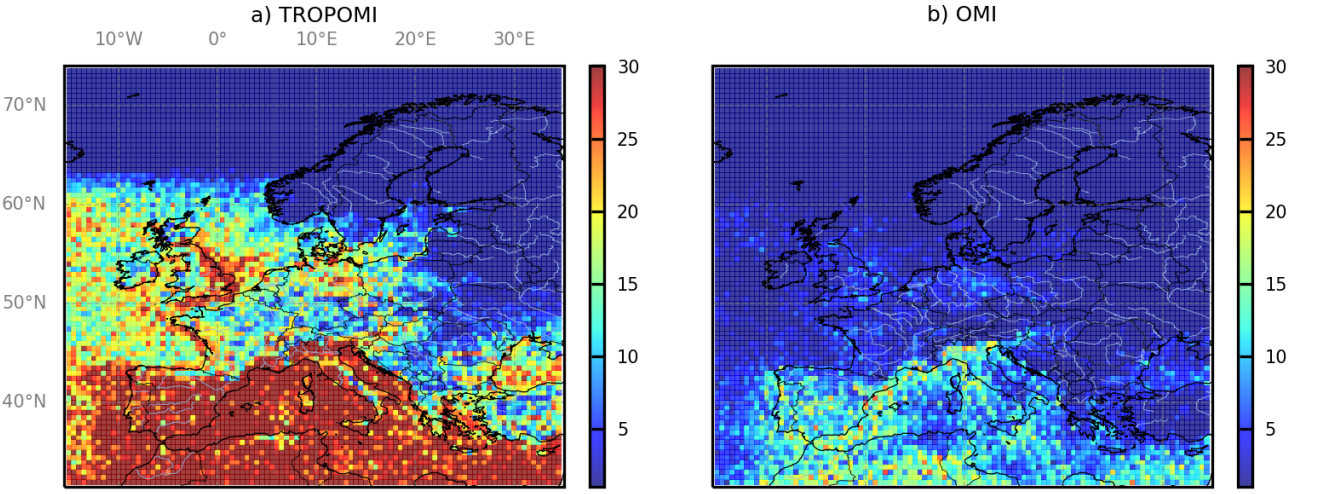


**Figure 5.** Monthly number of a) TROPOMI and b) OMI super-observations, in January 2019.

Various choices can be made for the derivation of the error associated with each super-observation. First, the error associated with each super-observation can be derived from the observation closest to the mean value, as in Plauchu et al. (2024). In this case, the derivation of the error associated with each super-observation, referred as **"OMI-conservative" or "TROPOMI-conservative"** in the following, is conservative compared to other studies where the super-observation uncertainty is reduced compared to that of individual observations (Boersma et al., 2016). The reduction of uncertainty when combining several observations accounts for the fact that the retrieval errors include random noise (in particular, instrumental noise without spatial correlation, i.e. errors which are independent from one observation to the other). However, OMI or TROPOMI $NO_2$ observa-

tions probably bear systematic errors from the instrument and from the retrieval process, which can exhibit important spatial correlations (Rijsdijk et al., 2024). This can justify a conservative attribution of observation errors to the super-observations. Nevertheless, in addition to this configuration, we have also performed a sensitivity test, referred to as **"OMI-optimistic" or "TROPOMI-optimistic"** in the following (Table 1), where the error associated with each super-observation is derived as the error from the observation closest to the mean value multiplied by a factor of $\frac{1}{\sqrt{nbobs}}$ , where $nbobs$ is the number of observations within a super-observation. In this case, the corresponding super-observation error is smaller than that of the individual observations.

### 2.5 Variational inversion of the $NO_x$ emissions

**The principle of our atmospheric inversions is to correct prior emission maps from the TNO-GHGco-v3 gridded inventory for the year 2005 (presented in Section 2.2) and initial conditions, by reducing differences between CHIMERE simulations and OMI-QA4ECV or TROPOMI-RPRO-v02.04 satellite data for the year 2019 as shown in Figure 1, using a variational inversion framework similar to that of Plauchu et al. (2024). Our new emission estimates are called "posterior" in the following.** 1-month inversion windows — independent from each other — have been performed over the entire year 2019. For each inversion window, the posterior estimate of the emissions is found by iteratively minimizing the cost function $J(\mathbf{x})$:

$$J(\mathbf{x}) = \frac{1}{2}(\mathbf{x}-\mathbf{x}^b)^T\mathbf{B}^{-1}(\mathbf{x}-\mathbf{x}^b) + \frac{1}{2}(\mathcal{H}(\mathbf{x})-\mathbf{y})^T\mathbf{R}^{-1}(\mathcal{H}(\mathbf{x})-\mathbf{y})$$

where $\mathbf{x}$, $\mathcal{H}$, $\mathbf{y}$, $\mathbf{B}$, $\mathbf{R}$ are respectively the control vector, the observation operator, the satellite observations, the prior error covariance matrix and the observation error covariance matrix. As in Plauchu et al. (2024), the definition of $\mathbf{x}$ ensures that the inversion solves separately for the two main types of NO emissions: the anthropogenic and the biogenic emissions (without any further sectorization or decomposition into more detailed emission components) and for the anthropogenic $NO_2$ emissions. With such a control vector, the prior NO/$NO_2$ anthropogenic emission ratio speciation from the GENEMIS recommendations (see Section 2.2) is not kept by the inversion. The analysis in the following focuses on the $NO_x$ emissions as the sum of the NO and $NO_2$ emissions.

Contrarily to Fortems-Cheiney et al. (2021b), and as in Plauchu et al. (2024), the prior uncertainty in both the anthropogenic and biogenic $NO_x$ emissions are characterized with log-normal distributions, allowing the inversion system to apply high variations in $NO_x$ emissions while ensuring that the inversion keeps the emissions positive, unlike the classic corrections of the emissions with scaling factors. Details about this feature are given in Plauchu et al. (2024).

Our control vector $\mathbf{x}$ contains:

- the logarithms of the scaling coefficients for NO anthropogenic emissions at a 1-day temporal resolution, at a 0.5°×0.5° (longitude, latitude) horizontal resolution and over the first 8 vertical levels of CHIMERE i.e, for each of the corresponding 101×85×8 grid cells,
- the logarithms of the scaling coefficients for $NO_2$ anthropogenic emissions at the same temporal and spatial resolutions as for NO,

– the logarithms of the scaling coefficients for NO biogenic emissions at a 1-day temporal resolution, at a 0.5°×0.5° (longitude, latitude) resolution and at the surface (over 1 vertical level only), i.e. for each of the corresponding 101×85×1 grid cells,

– factors scaling the NO and $NO_2$ 3D initial conditions at 0:00 UTC the first day of each month, at a 0.5°×0.5° (longitude, latitude) resolution and over the 17 vertical levels of CHIMERE.

The uncertainties in the observations **y** together with those in the observation operator $\mathcal{H}$, and the uncertainties in the prior estimate of the control vector **x** are assumed to have a Gaussian distribution Here, the first block of **B** corresponds to the logarithms of the anthropogenic flux factors. Each diagonal element is set at $(0.5)^2$: this variance value in the log-space corresponds to a factor ranging between 60%-164% in the emission space at the 1-day and model's grid scale. A second block is set for biogenic fluxes. On the diagonal, uncertainties are also set to a value of $(0.5)^2$, also corresponding to a factor ranging between 60%-164% in the emission space at the 1-day and model's grid scale. We account for spatial correlations in the uncertainties both for the anthropogenic and the natural parts. Spatial correlations are described by exponentially decaying functions with an e-folding length of 50 km over land and over the sea. Finally, in the third block of **B** for initial conditions, the variances are set at 20%.

The variance of the observation errors corresponding to individual super-observations in **R** is the quadratic sum of the error we have assigned to the OMI or TROPOMI super-observations, and of an estimate of the errors from the observation operator. We assume that the observation operator error is dominated by the chemistry-transport modeling error: it is set at 20% of the retrieval value, as in Fortems-Cheiney et al. (2021b). The monthly averages of the observation errors in **R** are shown in Figure 6 for the different configurations associated with the errors assigned to the OMI or TROPOMI super-observations (see Section 2.4.3). It is interesting to note that the TROPOMI-conservative configuration, ignoring the number of observations to reduce the error associated with the super-observation, presents lower errors than the OMI-conservative one. This is explained by the better signal-to-noise ratio of TROPOMI compared to OMI (van Geffen et al., 2022b).

The different experiments performed in this study are presented in Table 1. The inversions are conducted using the variational mode of the CIF with the limited-memory quasi-Newton minimisation algorithm M1QN3 (Gilbert and Lemaréchal, 1989) for the minimization of the cost function $J$. At each iteration of this minimization, the CIF uses a CHIMERE simulation to compute $J$ for a new estimate of **x** and the adjoint code of CHIMERE to compute the gradient of $J$ for this new estimate of **x**. We impose a reduction of the norm of the gradient of $J$ by 90% as a constraint for the interruption of the minimization process but the reduction of the norm of the gradient of $J$ actually often exceeds 95%.

## 3 Results

### 3.1 Comparison between OMI and TROPOMI super-observations

The $NO_2$ TVCDS from OMI-QA4ECV and older versions of the TROPOMI products have been compared in the literature. Sekiya et al. (2022) reported lower concentrations in TROPOMI unofficial reprocessing product (version 1.2 beta) than in OMI-

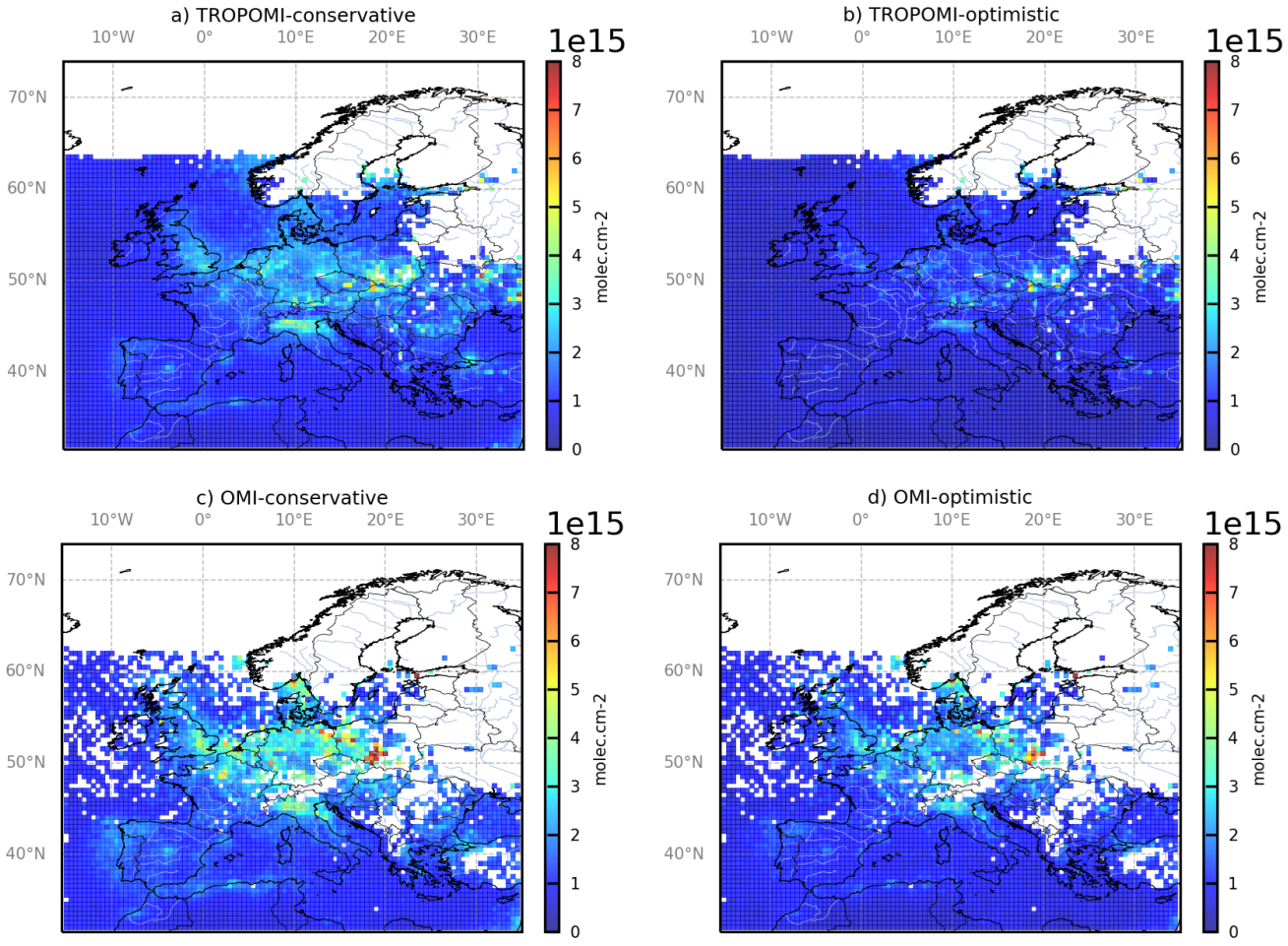


**Figure 6.** Monthly averages of the observation errors in **R** for the a) TROPOMI-conservative, b) TROPOMI-optimistic, c) OMI-conservative and d) OMI-optimistic configurations, in molec.cm$^{-2}$, for January 2019. The color scale is the same as for Figure 7. The observation errors in **R** include errors corresponding to the satellite retrievals and to the observation operator.

QA4ECV by 15% during April–May 2018 averaged over 60°S–60°N. As mentioned in the introduction, Lambert et al. (2021) reported $NO_2$ TVCDs from TROPOMI version 01.02 and 01.03 products systematically lower than from OMI-QA4ECV, with differences in terms of monthly $NO_2$ average reaching -40% over polluted regions in winter. Nevertheless, comparisons of TROPOMI-v01.04 with OMI-QA4ECV observations show an improved consistency between the two retrievals. Over Europe, while the bias was of about -17% in January 2019 with version 01.03, it was of about -4% in January 2020 with version 01.04 (Lambert et al., 2021). Here, we would like to characterize the consistencies between OMI-QA4ECV and TROPOMI-RPRO-v02.04, the more recent re-processing of the TROPOMI data.

OMI $NO_2$ and TROPOMI $NO_2$ super-observations present consistent geographical patterns (Fig. 7) with high concentrations

**Table 1.** Description of the inversions performed in this study.

| Name | Prior inventory | Satellite observations | Choice for the super-observation errors |
|---|---|---|---|
| OMI-conservative | TNO-GHGco-v3 for year 2005 | OMI-QA4ECV for year 2019 | conservative |
| TROPOMI–conservative | TNO-GHGco-v3 for year 2005 | TROPOMI-RPRO-v02.04 for year 2019 | conservative |
| OMI-optimistic | TNO-GHGco-v3 for year 2005 | OMI-QA4ECV for year 2019 | optimistic |
| TROPOMI-optimistic | TNO-GHGco-v3 for year 2005 | TROPOMI-RPRO-v02.04 for year 2019 | optimistic |
| OMI-obs2005 | TNO-GHGco-v3 for January 2005 | OMI-QA4ECV for January 2005 | optimistic |
| OMI-prior2019 | TNO-GHGco-v3 for January 2019 | OMI-QA4ECV for January 2019 | optimistic |

over emission hot spots. However, the average magnitude of the $NO_2$ TVCDs is different. The $NO_2$ TVCDs in the OMI-QA4ECV product are often higher than in the TROPOMI-RPRO-v02.04 product (Fig. 7a vs Fig. 7d, Fig. 8), with a mean difference between the two products over the entire domain of about +15% in January 2019 (Fig. 7g). It could be explained by the fact that TROPOMI underestimates the $NO_2$ TVCDs over highly polluted areas. The last evaluation of the TROPOMI-RPRO-v02.04 product around the world still indicates significant biases of TROPOMI $NO_2$ TVCDs of typically +13% over clean areas to -40% over highly polluted areas (Lambert et al., 2023; van Geffen et al., 2022b), even if these bias estimates are reduced when MAX-DOAS profile data are vertically smoothed using the TROPOMI AKs.

Since the OMI and TROPOMI AKs are different, and since the spatio-temporal samplings of the two data sets are also different, **a direct comparison between the OMI and TROPOMI datasets could be complex or misleading. The confrontation of the OMI retrievals to CHIMERE in the one hand, and of the TROPOMI retrievals to CHIMERE in the other hand can be used as an indirect but more suitable comparison between the OMI and TROPOMI datasets.** Interestingly, while the mean $NO_2$ TVCDs observed by OMI is higher by about +15% than the one observed by TROPOMI, the mean CHIMERE-OMI $NO_2$ TVCDs is lower by about 7% compared to the CHIMERE-TROPOMI ones over the entire domain in January 2019 (Fig. 7h). It can be explained by the fact that the AKs in TROPOMI-RPRO-v02.04 tend to be larger above the first four levels than in OMI-QA4ECV (Figure 3).

### 3.2 Comparison between satellite super-observations and prior CHIMERE simulations

The CHIMERE-OMI and the CHIMERE-TROPOMI simulations, based on the TNO-GHGco-v3 inventory for the year 2005, both present higher $NO_2$ TVCDs than the OMI and TROPOMI super-observations for the year 2019 (Fig. 7). This is expected since the $NO_x$ anthropogenic emissions have been decreased in Europe since 2005 (EEA, 2021). However, the magnitude of

the discrepancies between the simulations and the satellite super-observations vary. For example, in January 2019 over the entire domain, the simulated CHIMERE-TROPOMI TVCDs are about 38% higher than TROPOMI super-observations while simulated CHIMERE-OMI TVCDs are about 23% higher than the OMI ones. Over the most polluted area, including parts of Western and Central Europe (0°E-20°E; 40°N-60°N, see the purple box in Fig. 7), the simulated CHIMERE-TROPOMI and CHIMERE-OMI also present a strong positive relative difference of about +39% compared to TROPOMI and of about +29% compared to OMI respectively. TROPOMI therefore shows a stronger drop in the $NO_2$ TVCDs than OMI and consequently, the TROPOMI inversions would lead to lower $NO_x$ anthropogenic emissions than the OMI inversions.

The highest differences between the super-observations and the CHIMERE-OMI or CHIMERE-TROPOMI simulations are found in autumn and in winter, and particularly for the months of January, November and December (Fig. 8). It can be deduced that the winter European $NO_2$ simulated TVCDs will be decreased both by the OMI and the TROPOMI inversions, even if the respective corrections to the prior emissions will be different in magnitude. However, in spring and in summer (e.g., for the months of April, May, June, July and August), the monthly averages of the TROPOMI super-observations are always lower than the CHIMERE-TROPOMI $NO_2$ TVCDs while the monthly averages of the OMI super-observations remains close to the CHIMERE-OMI ones (Fig. 8b). The TROPOMI and OMI super-observations therefore will lead to different conclusions concerning the potential reductions of $NO_x$ anthropogenic emissions during spring and summer since 2005.

### 3.3 Improvement of the fit between satellite super-observations and CHIMERE simulations

The inversions bring the simulated $NO_2$ TVCDs closer to OMI or to TROPOMI super-observations (Fig. 8). In general, the reduction of the bias between the super-observations and the CHIMERE simulations is higher in winter than in summer (Fig. 8). **In January 2019 over the entire domain, the mean bias between the TROPOMI super-observations and the CHIMERE-TROPOMI simulations is reduced by about 70% with the conservative configuration (Section 2.4.3) while the mean bias is reduced by about 83% with the optimistic one. The mean bias between the OMI super-observations and the CHIMERE-OMI simulations is also reduced, by about 73% with the conservative configuration, while the mean bias is reduced by about 80% with the optimistic one.** The TROPOMI-optimistic and OMI-optimistic corrections are higher than the TROPOMI-conservative and OMI-conservative ones, respectively. It can be explained by the lower error associated to the "optimistic" super-observations, giving more weight to the satellite data, compared to the "conservative" ones (see Section 2.4.3).

To improve and optimize the fit between satellite super-observations and CHIMERE simulations the inversion system reduces the $NO_x$ anthropogenic emissions in the year 2019 (Fig. 9).

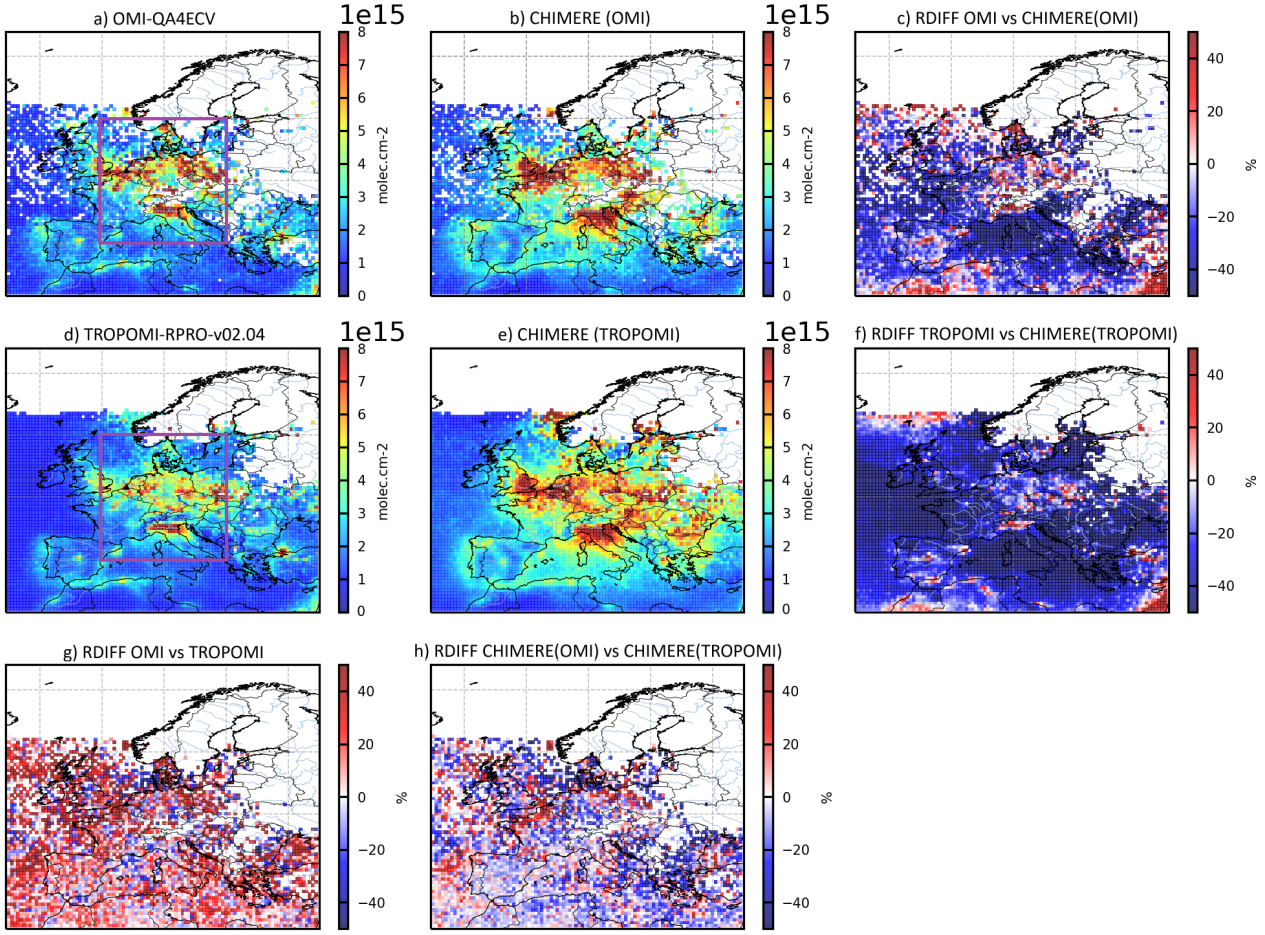


**Figure 7.** Monthly averages of $NO_2$ a) super-observations based on OMI and b) the CHIMERE-OMI simulation, where and when OMI-QA4ECV super-observations are available; d) super-observations based on TROPOMI-RPRO-v02.04 and e) CHIMERE-TROPOMI simulations, where and when TROPOMI super-observations are available, in molec.cm$^{-2}$. Monthly averages for January 2019 of the relative differences between c) the super-observations from OMI-QA4ECV $NO_2$ TVCDs and the CHIMERE-OMI simulation, f) the super-observations from TROPOMI $NO_2$ TVCDs and the CHIMERE-TROPOMI simulation, g) the OMI and TROPOMI super-observations and h) the CHIMERE-OMI and the CHIMERE-TROPOMI simulations, in %. The prior TNO-GHGco-v3 anthropogenic emission for the year 2005 are used to simulate the $NO_2$ TVCDs. The purple box shows Western and Central Europe (0°E-20°E; 40°N-60°N).

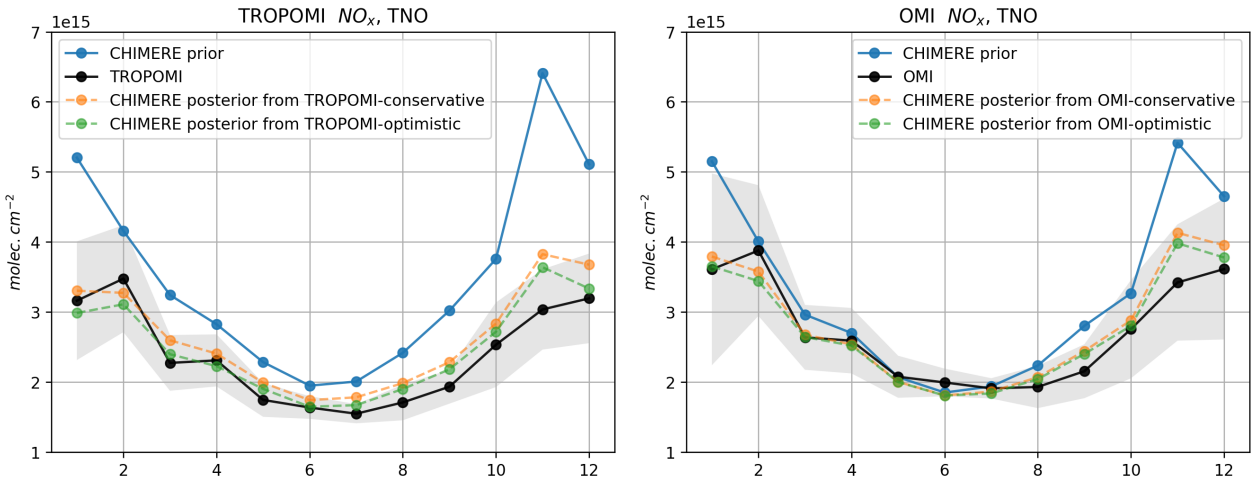


**Figure 8.** January to December 2019 times series of monthly averaged $NO_2$ TVCDs over Western and Central Europe (0°E-20°E; 40°N-60°N). Left: from TROPOMI-RPRO-v02.4 super-observations (in black) and the CHIMERE-TROPOMI prior (in blue), CHIMERE posterior from TROPOMI-conservative (in orange) and CHIMERE posterior from TROPOMI-optimistic (in green) simulations. Right: same as left but for OMI-QA4ECV super-observations, in molec.cm$^{-2}$. The prior simulations of TVCDs use TNO-GHGco-v3 anthropogenic emissions for the year 2005.

### 3.4 Posterior estimates of $NO_x$ European anthropogenic emissions in 2019: evaluation with comparisons to the TNO-GHGco-v3 inventory

As the anthropogenic emissions contribute to about 95% of the total $NO_x$ emissions in Europe even in summer (see Section 2.3), this section focuses on the inversion results in terms of comparisons between the prior anthropogenic $NO_x$ emissions for 2005 and the posterior emissions from the OMI and TROPOMI inversions for the year 2019 in the European Union + United Kingdom (EU-27+UK) area. Nevertheless, the inversion results do not seem to indicate missing sources in the biogenic emissions, even if we do not include a specific component of $NO_x$ emissions from agricultural soils in our prior estimate of $NO_x$ emissions (see Section 2.2). The annual budget for biogenic emissions are in fact only changed by a few percents both by the OMI and TROPOMI inversions (not shown).

The posterior emissions from the OMI and TROPOMI inversions are compared to the emission estimates from the TNO-GHGco-v3 inventory for the year 2019 (Tab. 3, Fig. 10). At the European scale (Fig. 10) and at the national scale (Tab. 3), both the posterior anthropogenic $NO_x$ emissions from the OMI and TROPOMI inversions for the year 2019 are lower than the prior ones for the year 2005.

When assimilating OMI-conservative super-observations, the $NO_x$ anthropogenic emissions for EU-27+UK and for Western Europe are decreased by about 13% and 17%, respectively, between 2005 and 2019 (Table 3). Similar results are obtained when assimilating OMI-optimistic super-observations (decrease by about 16% and 21%, respectively, Table 3). These decreases of emissions between 2005 and 2019 are higher than the decrease estimated by Miyazaki et al. (2017), finding a negative change of only -0.1% in Europe (defined as 10°W–30°E, 35–60°N in their study) and -8.8% in Western Europe between 2005 and 2014. However, the OMI-conservative and the OMI-optimistic posterior $NO_x$ emissions over EU-27+UK respectively remain +53% and +47% higher than the estimation of the TNO-GHGco-v3 inventory for 2019. To support the assumption that the positive bias between the CHIMERE simulations driven by the inventory for 2005 and the satellite observations in 2019 (seen in Figure 7) is mainly related to the decrease of the European emissions, we have performed two sensitivity tests for one month in January: the first, called "OMI-obs2005", uses CHIMERE simulations driven by the TNO inventory for 2005 and OMI observations for 2005 (Table 1), the second, called "OMI-prior2019", uses CHIMERE simulations driven by the TNO inventory for 2019 and OMI observations for 2019 (Table 1). In these cases, the $NO_x$ anthropogenic emissions for EU-27+UK in January 2005 and in January 2019 are both decreased by about 6% by the inversions (Table 2). Using the same configuration of the $\mathbf{R}$ covariance matrix, these corrections are much smaller than the correction of about -21% reached in the case OMI-optimistic for the month of January 2019 (Table 2, Figure 10), when using prior emissions from the TNO inventory for 2005 and OMI observations for 2019 (Table 1). This result therefore shows that the positive bias between the CHIMERE simulations driven by the inventory for 2005 and the satellite observations in 2019 is mainly due to the decline in European $NO_x$ emissions since 2005.

At the pixel scale both over urban and rural areas (Fig. 9) and at the national or European scales (Table 3, Fig. 10), the decreases of $NO_x$ anthropogenic emissions estimated from the OMI inversions between 2005 and 2019 are lower than from the TROPOMI ones. This can be explained by the fact that the relative differences between TROPOMI super-observations

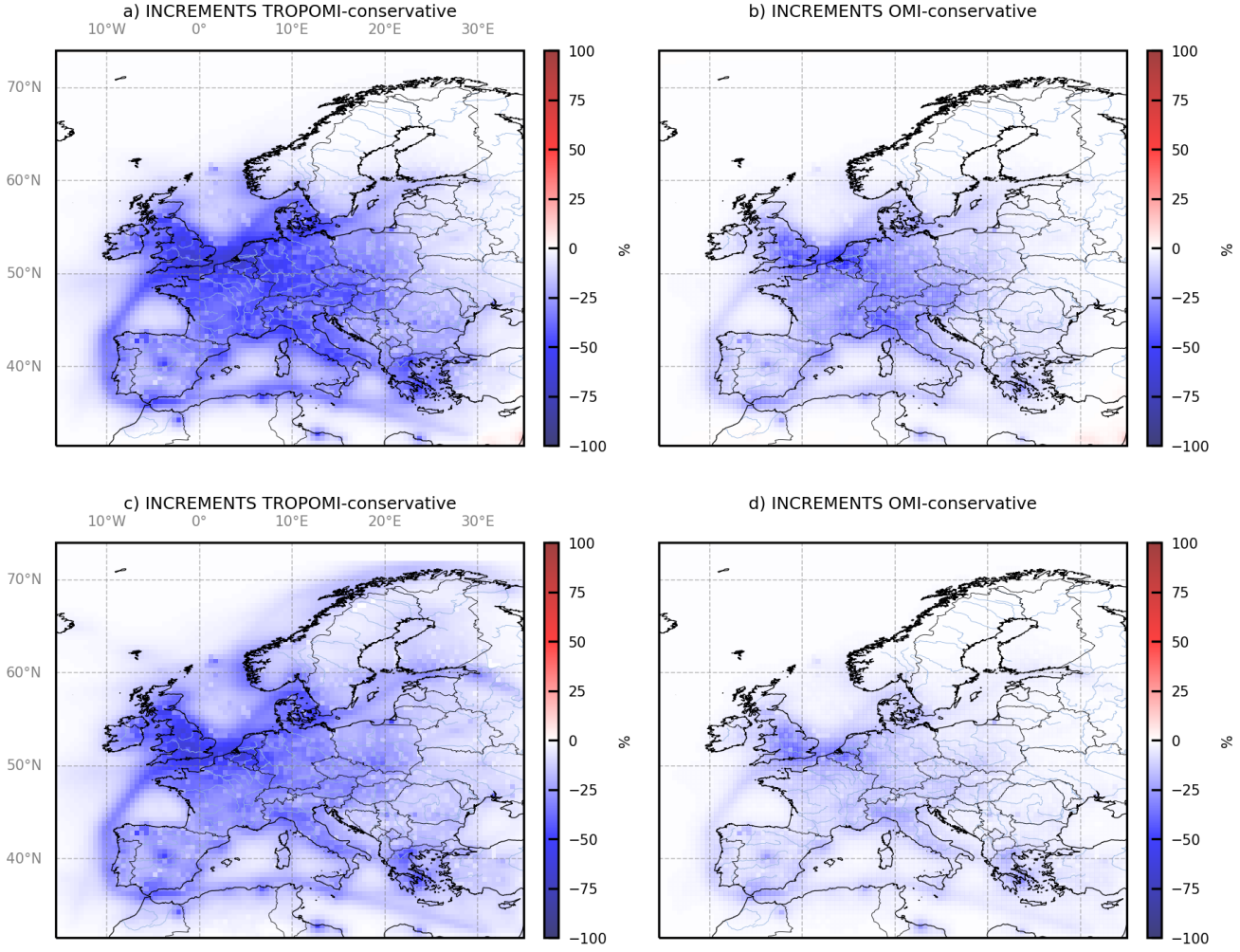


**Figure 9.** Monthly mean relative corrections to the prior $NO_x$ emissions for year 2005 from the a) TROPOMI-conservative and from the b) OMI-conservative inversions, calculated as (posterior-prior)/prior, in %, for top) the month of January 2019 and bottom) the entire year 2019.

**Table 2.** $NO_x$ anthropogenic emissions for EU-27+UK estimated from different sensitivity tests described in Table 1, in kteq$NO_2$, for the month of January 2005 or for the month of January 2019.

| Name of the inversions | Prior TNO-GHGco-v3 for January 2005 | Prior TNO-GHGco-v3 for January 2019 | Posterior using OMI-QA4ECV for January 2005 | Posterior using OMI-QA4ECV for January 2019 | Relative difference posterior-prior |
|---|---|---|---|---|---|
| TROPOMI-optimistic | 1257 | - | - | 661 | -47% |
| OMI-optimistic | 1257 | - | - | 993 | -21% |
| OMI-obs2005 | 1257 | - | 1180 | - | -6% |
| OMI-prior2019 | - | 736 | - | 696 | -6% |

and the CHIMERE-TROPOMI simulations are larger than between OMI super-observations and the CHIMERE-OMI ones (see Section 3.2), due to different cloud pressures and albedos affecting the averaging kernels (see Section 2.4.3). As OMI super-observations are closer to the CHIMERE-OMI simulations, particularly in spring and summer, the OMI inversions make lower corrections in the $NO_x$ anthropogenic emissions than the TROPOMI ones. This can also be explained by the fact that i) TROPOMI presents a better coverage compared to OMI, with a much larger number of observations (Figure 5) and ii) TROPOMI presents lower errors associated with its super-observations than OMI, even in the case where the error associated with the super-observation is not reduced depending on the number of observations (Figure 6).

Assimilating TROPOMI-conservative super-observations, the decrease of the $NO_x$ anthropogenic emissions for EU-27+UK and for Western Europe between 2005 and 2019 is indeed of about -32% and -42%, respectively. Assimilating TROPOMI-optimistic super-observations even lead to higher decreases with -45% and -54%, respectively, for EU-27+UK and for Western Europe. It can be explained by the lower error associated to the TROPOMI-optimistic super-observations, giving more weight to the satellite data, compared to the TROPOMI-conservative ones (see Section 2.4.3). The decrease in $NO_x$ emissions from the TROPOMI-conservative inversions ranges from -9% for Cyprus to -54% for Belgium, while it ranges from -22% for Montenegro to -63% for Belgium from the TROPOMI-optimistic ones. The TROPOMI-conservative posterior $NO_x$ emissions are closer to the TNO-GHGco-v3 inventory at the European scale compared to the OMI-conservative ones, but still with relative differences of about +19% for EU-27+UK. The TROPOMI-optimistic posterior emissions become consistent with the TNO-GHGco-v3 inventory, with a relative difference of only -2%.

Generally, the corrections provided by the inversions are stronger for Western and Southern countries than for Eastern or Northern ones (Table 3, Fig. 9). For example, the TROPOMI-optimistic posterior emissions suggest higher annual budgets in several Central or Eastern European countries (e.g., Slovakia, Slovenia, Croatia) than those provided by TNO, based on official country emission reporting. It may be due to the fact that $NO_2$ TVCDs (Krotkov et al., 2016; Fortems-Cheiney et al.,

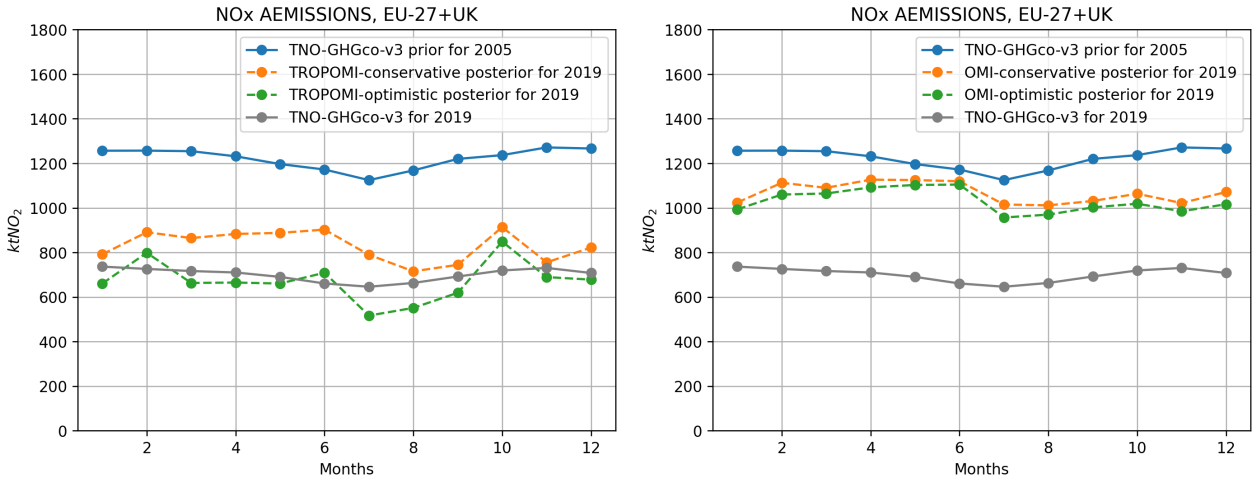


**Figure 10.** Left) January to December 2019 times series of monthly estimates of anthropogenic $NO_x$ prior emissions from the TNO-GHGco-v3 inventory for the year 2005 (in blue), posterior anthropogenic $NO_x$ emission estimates from the TROPOMI-conservative (in orange) and TROPOMI-optimistic (in green) inversions, in kteq$NO_2$, for the EU-27+UK area. Right) same as left, but for posterior anthropogenic $NO_x$ emission estimates from the OMI-conservative (in orange) and OMI-optimistic (in green) inversions.

2021a) and the $NO_x$ emissions in these countries have not strongly decreased since 2005. It can also be explained by the cloud coverage limiting the number of satellite data over these countries (Figure 5). When the coverage of a country by OMI or TROPOMI super-observations is sparse, the posterior emissions indeed remain close to the prior emission estimates i.e. at their 2005 level. On the contrary, the TROPOMI-optimistic inversions show lower annual budgets over Western European countries such as Belgium and the Netherlands than TNO (Table 3), suggesting that $NO_x$ emissions could have been more reduced than officially reported in these countries.

Table 3: National anthropogenic prior $NO_x$ emission estimates from the TNO-GHGco-v3 inventory for the year 2005 and relative increments provided by the different inversions in %, for the year 2019. The relative differences between emission estimates of the TNO-GHGco-v3 anthropogenic for the year 2019 against year 2005 are given for information.

| Country | Prior TNO-GHGco-v3 2005 | Increments from the TROPOMI-conservative inversion | Increments from the TROPOMI-optimistic inversion | Increments from the OMI-conservative inversion | Increments from the OMI-optimistic inversion | Rdiff TNO 2019 vs 2005 |
|---|---|---|---|---|---|---|
| | kteq$NO_2$ | % | % | % | | % |
| Albania | 32 | -19 | -36 | -7 | -10 | 4 |

.../...

| Country | Prior TNO-GHGco-v3 2005 | Increments from the TROPOMI-conservative inversion | Increments from the TROPOMI-optimistic inversion | Increments from the OMI-conservative inversion | Increments from the OMI-optimistic inversion | Rdiff TNO 2019 vs 2005 |
|---|---|---|---|---|---|---|
| | $kteqNO_2$ | % | % | % | % | % |
| Austria | 224 | -30 | -43 | -12 | -15 | -42 |
| Belgium | 359 | -54 | -63 | -27 | -31 | -47 |
| Bulgaria | 175 | -15 | -29 | -5 | -7 | -47 |
| Bosnia-Herzegovina | 53 | -13 | -24 | -4 | -6 | -27 |
| Croatia | 116 | -19 | -32 | -6 | -9 | -40 |
| Switzerland | 88 | -30 | -41 | -13 | -16 | -35 |
| Cyprus | 52 | -9 | -22 | -4 | -6 | -33 |
| Czech Republic | 271 | -27 | -37 | -9 | -11 | -45 |
| Germany | 1704 | -34 | -44 | -13 | -15 | -32 |
| Denmark | 346 | -37 | -49 | -11 | -13 | -47 |
| Spain | 1670 | -29 | -46 | -12 | -16 | -49 |
| Estonia | 82 | -20 | -30 | -4 | -5 | -32 |
| Finland | 239 | -15 | -24 | -3 | -3 | -42 |
| France | 1747 | -34 | -48 | -12 | -16 | -48 |
| United Kingdom | 2049 | -48 | -59 | -20 | -23 | -50 |
| Greece | 834 | -27 | -45 | -12 | -17 | -43 |
| Hungary | 161 | -22 | -34 | -7 | -10 | -38 |
| Ireland | 171 | -27 | -41 | -5 | -7 | -46 |
| Italy | 1575 | -26 | -41 | -12 | -15 | -47 |
| Lithuania | 59 | -14 | -23 | -2 | -3 | -25 |
| Latvia | 55 | -13 | -23 | -2 | -3 | -30 |
| Montenegro | 11 | -11 | -22 | -3 | -5 | -22 |
| Netherlands | 583 | -48 | -55 | -23 | -25 | -40 |
| Norway | 308 | -24 | -36 | -4 | -5 | -32 |
| Poland | 811 | -24 | -33 | -6 | -8 | -19 |
| Portugal | 515 | -23 | -42 | -8 | -12 | -43 |
| Romania | 314 | -15 | -27 | -4 | -6 | -31 |
| Serbia | 170 | -22 | -36 | -8 | -11 | -39 |
| Slovakia | 102 | -21 | -31 | -7 | -9 | -43 |

…/…

| Country | Prior TNO-GHGco-v3 2005 | Increments from the TROPOMI-conservative inversion | Increments from the TROPOMI-optimistic inversion | Increments from the OMI-conservative inversion | Increments from the OMI-optimistic inversion | Rdiff TNO 2019 vs 2005 |
|---|---|---|---|---|---|---|
| | $kteqNO_2$ | % | % | % | % | % |
| Slovenia | 60 | -24 | -38 | -9 | -12 | -47 |
| Sweden | 315 | -24 | -35 | -6 | -7 | -36 |
| Turkey | 660 | -13 | -25 | -5 | -7 | -16 |
| Ukraine | 511 | -14 | -25 | -4 | -5 | -33 |
| Benelux | 955 | -50 | -58 | -24 | -27 | -43 |
| Western Europe | 4922 | -42 | -54 | -17 | -21 | -48 |
| Central Europe | 3361 | -30 | -40 | -11 | -13 | -32 |
| Northern Europe | 1403 | -25 | -36 | -6 | -7 | -38 |
| Southern Europe | 5365 | -25 | -42 | -11 | -14 | -46 |
| Eastern Europe | 1238 | -19 | -28 | -5 | -6 | -32 |
| EU-27+UK | 14655 | -32 | -45 | -13 | -16 | -43 |

## 4 Conclusion

There are great expectations about the detection and the quantification of $NO_x$ emissions using $NO_2$ TVCDs from satellite observations and inverse systems. This study assesses the potential of the OMI-QA4ECV and TROPOMI satellite observations to improve the knowledge on European $NO_x$ emissions at the regional scale and to inform about the spatio-temporal variability of $NO_x$ emissions **in 2019 compared to 2005**, at the resolution of 0.5° over Europe. Starting from European emission estimates from the TNO-GHGco-v3 inventory for the year 2005, regional inversions using the CIF coupled to CHIMERE CTM and assimilating satellite $NO_2$ TVCDs from OMI and TROPOMI have been performed to estimate the European annual and seasonal budgets for the year 2019.

**As the anthropogenic emissions strongly contribute to the total $NO_x$ emissions in Europe even in summer, we assume that the differences between the 2005 and the 2019 budgets are mainly due to anthropogenic emissions and not to the biogenic ones. However, the level of distinction between the anthropogenic and biogenic emissions in the inversions is one of the sources of uncertainty in the estimate of the anthropogenic emissions. The corrections provided by the inversions to the prior emissions can also be limited by the cloud coverage affecting the OMI or TROPOMI observations, by errors in the OMI or TROPOMI data and by errors in the CTM. Finally, the set-up of error covariance matrices could also have a strong impact on the emission estimates resulting from the inversions.**

Both the OMI and TROPOMI inversions show decreases in European $NO_x$ anthropogenic emission budgets **in 2019 compared to 2005**. Nevertheless, the magnitude of the reductions of the $NO_x$ anthropogenic emissions are different with OMI and TROPOMI data, with decreases in EU-27+UK between 2005 and 2019 of 16% and 45% respectively. The decrease of $NO_x$ anthropogenic emissions estimated from the TROPOMI inversions are substantially higher than from the OMI inversions. This is mainly explained by i) the fact that the differences between CHIMERE-TROPOMI simulations and the TROPOMI super-observations are larger than between CHIMERE-OMI and OMI super-observations, due to different AKs, ii) the better coverage of TROPOMI compared to OMI and iii) the lower errors associated with the TROPOMI super-observations compared to OMI.

The TROPOMI-optimistic inversions, giving weight to the satellite data, become consistent with the independent TNO-GHGco-v3 inventory for the year 2019, with annual budgets for EU-27+UK showing absolute relative difference of only 2%. These TROPOMI inversions are therefore in agreement with the magnitude of the decline in $NO_x$ emissions declared by countries, when aggregated at the European scale.

Our results —with OMI and TROPOMI data leading to different magnitudes of corrections on $NO_x$ anthropogenic emissions —suggest that more observational constraints would be required to sharpen the European emission estimates. Observational information from future satellite missions such as Sentinel-4 on board geostationary satellites would increase the number of observations for better constraining the $NO_x$ emissions in particular for Eastern and Northern countries.

## 5 Author contributions

AFC and GB conceptualized the study and carried out the results analysis. AFC carried out the inversions. EP, RP, AB, IP and AM developed the CIF inversion system, including preprocessing for fluxes and satellite observations. HDvdG and SD provided the TNO-GHGco-v3 inventory used as prior emissions in this study. ASP designed parts of Figure 1. All the co-authors contributed to writing the manuscript.

## 6 Data availability

OMI-QA4ECV data are freely available through the website www.qa4ecv.eu and http://temis.nl/qa4ecv/no2.html, (Boersma et al., 2017). TROPOMI-RPRO-v02.04 data are freely available through the website https://identity.dataspace.copernicus.eu. The TNO-GHGco-v3 inventory (Super et al., 2020) is available upon request from TNO (contact: Hugo Denier van der Gon, hugo.deniervandergon@tno.nl).

## 7 Code availability

The CHIMERE code is available here: http://www.lmd.polytechnique.fr/chimere/ (Menut et al., 2013; Mailler et al., 2017). The CIF inversion system (Berchet et al., 2021) is available at https://doi.org/10.5281/zenodo.6304912 (Berchet et al., 2022).

## 8 Financial support

A large part of the development and analysis were conducted in the frame of the H2020 VERIFY and COCO2 projects, funded by the European Commission Horizon 2020 research and innovation programme, respectively under agreement number 776810 and 958927, and in the frame of the World Emission project funded by the European Space Agency. This study has received funding from the French ANR project ARGONAUT under grant agreement No ANR-19-CE01-0007 and from the French PRIMEQUAL project LOCKAIR under grant agreement No 2162D0010. This work was also supported by the CNES (Centre National d'Etudes Spatiales), in the frame of the TOSCA ARGOS project.

## 9 Acknowledgements

We acknowledge the OMI-QA4ECV and the TROPOMI group for the production of the $NO_2$ retrievals. We wish to thank all the persons involved in the preparation, coordination and management of the H2020 VERIFY and COCO2 projects, as well as the ESA World Emission project. This work was granted access to the HPC resources of TGCC under the allocations A0140102201 made by GENCI. Finally, we wish to thank Julien Bruna (LSCE) and his team for computer support.

## 10 Competing Interests

The authors declare that they have no conflict of interest.

## References


Aumont, B., Chervier, F., and Laval, S.: Contribution of HONO sources to the NOx/HOx/O3 chemistry in the polluted boundary layer, Atmospheric Environment, 37, 487–498, https://doi.org/https://doi.org/10.1016/S1352-2310(02)00920-2, 2003.

Berchet, A., Sollum, E., Thompson, R. L., Pison, I., Thanwerdas, J., Broquet, G., Chevallier, F., Aalto, T., Berchet, A., Bergamaschi, P., Brunner, D., Engelen, R., Fortems-Cheiney, A., Gerbig, C., Groot Zwaaftink, C. D., Haussaire, J.-M., Henne, S., Houweling, S., Karstens, U., Kutsch, W. L., Luijkx, I. T., Monteil, G., Palmer, P. I., van Peet, J. C. A., Peters, W., Peylin, P., Potier, E., Rödenbeck, C., Saunois, M., Scholze, M., Tsuruta, A., and Zhao, Y.: The Community Inversion Framework v1.0: a unified system for atmospheric inversion studies, Geoscientific Model Development, 14, 5331–5354, https://doi.org/10.5194/gmd-14-5331-2021, 2021.

Berchet, A., Sollum, E., Pison, I., Thompson, R. L., Thanwerdas, J., Fortems-Cheiney, A., van Peet, J. C. A., Potier, E., Cheval-lier, F., and Broquet, G.: The Community Inversion Framework: codes and documentation (v1.1), Tech. rep., https://doi.org/https://doi.org/10.5281/zenodo.6304912, 2022.

Bieser, J., Aulinger, A., Matthias, V., Quante, M., and Denier van der Gon, H.: Vertical emission profiles for Europe based on plume rise calculations, Environmental Pollution, 159, 2935–2946, https://doi.org/https://doi.org/10.1016/j.envpol.2011.04.030, nitrogen Deposition, Critical Loads and Biodiversity, 2011.

Boersma, K., Vinken, G., and Eskes, H.: Representativeness errors in comparing chemistry transport and chemistry climate models with satellite UV–Vis tropospheric column retrievals, Geoscientific Model Development, 9, 875–898, 2016.

Boersma, K., , van Geffen, G., Eskes, H., van der A, R., De Smedt, I., Van Roozendael, M., Yu, H., Richter, A., Peters, E., Beirle, S., Wagner, T., Lorente, A., Scanlon, T., Compernoelle, S., and Lambert, J.-C.: Product Specification Document for the QA4ECV NO2 ECV precursor product, techreport QA4ECV Deliverable D4.6, Tech. rep., http://www.qa4ecv.eu/sites/default/files/D4.6.pdf, 2017.

Boersma, K. F., Eskes, H. J., and Brinksma, E. J.: Error analysis for tropospheric NO2 retrieval from space, Journal of Geophysical Research: Atmospheres, 109, https://doi.org/https://doi.org/10.1029/2003JD003962, 2004.

Boersma, K. F., Jacob, D. J., Eskes, H. J., Pinder, R. W., Wang, J., and van der A, R. J.: Intercomparison of SCIAMACHY and OMI tropospheric NO2 columns: Observing the diurnal evolution of chemistry and emissions from space, Journal of Geophysical Research: Atmospheres, 113, https://doi.org/https://doi.org/10.1029/2007JD008816, 2008.

Boersma, K. F., Eskes, H. J., Richter, A., De Smedt, I., Lorente, A., Beirle, S., van Geffen, J. H. G. M., Zara, M., Peters, E., Van Roozendael, M., Wagner, T., Maasakkers, J. D., van der A, R. J., Nightingale, J., De Rudder, A., Irie, H., Pinardi, G., Lambert, J.-C., and Compernolle, S. C.: Improving algorithms and uncertainty estimates for satellite $NO_2$ retrievals: results from the quality assurance for the essential climate variables (QA4ECV) project, Atmospheric Measurement Techniques, 11, 6651–6678, https://doi.org/10.5194/amt-11-6651-2018, 2018.

Bovensmann, H., Burrows, J. P., Buchwitz, M., Frerick, J., Noël, S., Rozanov, V. V., Chance, K. V., and Goede, A. P. H.: SCIAMACHY: Mission Objectives and Measurement Modes, Journal of the Atmospheric Sciences, 56, 127 – 150, https://doi.org/https://doi.org/10.1175/1520-0469(1999)056<0127:SMOAMM>2.0.CO;2, 1999.

Burrows, J., Hölzle, E., Goede, A., Visser, H., and Fricke, W.: SCIAMACHY—scanning imaging absorption spectrometer for atmospheric chartography, Acta Astronautica, 35, 445–451, https://doi.org/https://doi.org/10.1016/0094-5765(94)00278-T, earth Observation, 1995.

Burrows, J. P., Weber, M., Buchwitz, M., Rozanov, V., Ladstätter-Weißenmayer, A., Richter, A., DeBeek, R., Hoogen, R., Bramstedt, K., Eichmann, K.-U., Eisinger, M., and Perner, D.: The Global Ozone Monitoring Experiment (GOME): Mission Con-

cept and First Scientific Results, Journal of the Atmospheric Sciences, 56, 151 – 175, https://doi.org/https://doi.org/10.1175/1520-0469(1999)056<0151:TGOMEG>2.0.CO;2, 1999.

Castellanos, P. and Boersma, K.: Reductions in nitrogen oxides over Europe driven by environmental policy and economic recession, Scientific Reports, 2, https://doi.org/https://doi.org/10.1038/srep00265, 2012.

Dellaert, S. N., Visschedijk, A., Kuenen, J., Super, I., and Denier van der Gon, H.: Final High Resolution emission data 2005-2018, Tech. rep., https://verify.lsce.ipsl.fr/images/PublicDeliverables/VERIFY_D2_3_TNO_v1.pdf, 2021.

Derognat, C., Beekmann, M., Baeumle, M., Martin, D., and Schmidt, H.: Effect of biogenic volatile organic compound emissions on tropospheric chemistry during the Atmospheric Pollution Over the Paris Area (ESQUIF) campaign in the Ile-de-France region, Journal of Geophysical Research: Atmospheres, 108, 2003.

Ding, J., Miyazaki, K., van der A, R. J., Mijling, B., Kurokawa, J.-i., Cho, S., Janssens-Maenhout, G., Zhang, Q., Liu, F., and Levelt, P. F.: Intercomparison of $NO_x$ emission inventories over East Asia, Atmospheric Chemistry and Physics, 17, 10 125–10 141, https://doi.org/10.5194/acp-17-10125-2017, publisher: Copernicus GmbH, 2017.

EEA: Air quality in Europe — 2021 report, Sources and Emissions of air pollutants in Europe, Tech. rep., European Union, https://doi.org/10.2800/549289, 2021.

EEA: Air quality in Europe 2021, Tech. rep., https://www.eea.europa.eu/publications/air-quality-in-europe-2021, 2022.

EEA: Air quality in Europe 2022, Tech. rep., https://doi.org/10.2800/488115, 2023.

Eskes, H. J. and Boersma, K. F.: Averaging kernels for DOAS total-column satellite retrievals, Atmospheric Chemistry and Physics, 3, 1285–1291, https://doi.org/10.5194/acp-3-1285-2003, 2003.

Fortems-Cheiney, A., Broquet, G., Pison, I., Saunois, M., Potier, E., Berchet, A., Dufour, G., Siour, G., Denier van der Gon, H., Dellaert, S. N. C., and Boersma, K. F.: Analysis of the Anthropogenic and Biogenic NOx Emissions Over 2008–2017: Assessment of the Trends in the 30 Most Populated Urban Areas in Europe, Geophysical Research Letters, 48, e2020GL092 206, https://doi.org/https://doi.org/10.1029/2020GL092206, e2020GL092206 2020GL092206, 2021a.

Fortems-Cheiney, A., Pison, I., Broquet, G., Dufour, G., Berchet, A., Potier, E., Coman, A., Siour, G., and Costantino, L.: Variational regional inverse modeling of reactive species emissions with PYVAR-CHIMERE-v2019, Geoscientific Model Development, 14, 2939–2957, https://doi.org/10.5194/gmd-14-2939-2021, 2021b.

Fortems-Cheiney, A., Broquet, G., Potier, E., Plauchu, R., Berchet, A., Pison, I., Denier van der Gon, H., and Dellaert, S.: CO anthropogenic emissions in Europe from 2011 to 2021: insights from Measurement of Pollution in the Troposphere (MOPITT) satellite data, Atmospheric Chemistry and Physics, 24, 4635–4649, https://doi.org/10.5194/acp-24-4635-2024, 2024.

Georgoulias, A. K., van der A, R. J., Stammes, P., Boersma, K. F., and Eskes, H. J.: Trends and trend reversal detection in 2 decades of tropospheric $NO_2$ satellite observations, Atmospheric Chemistry and Physics, 19, 6269–6294, https://doi.org/10.5194/acp-19-6269-2019, 2019.

Gilbert, J. and Lemaréchal, C.: Some numerical experiments with variable storage quasi Newton algorithms, Math. Program., 45, 407–435, https://doi.org/10.1007/BF01589113, 1989.

Guenther, A., Karl, T., Harley, P., Wiedinmyer, C., Palmer, P. I., and Geron, C.: Estimates of global terrestrial isoprene emissions using MEGAN (Model of Emissions of Gases and Aerosols from Nature), Atmospheric Chemistry and Physics, 6, 3181–3210, https://doi.org/10.5194/acp-6-3181-2006, 2006.

Kleipool, Q. L., Dobber, M. R., de Haan, J. F., and Levelt, P. F.: Earth surface reflectance climatology from 3 years of OMI data, Journal of Geophysical Research: Atmospheres, 113, https://doi.org/https://doi.org/10.1029/2008JD010290, 2008.

Krotkov, N. A., McLinden, C. A., Li, C., Lamsal, L. N., Celarier, E. A., Marchenko, S. V., Swartz, W. H., Bucsela, E. J., Joiner, J., Duncan, B. N., Boersma, K. F., Veefkind, J. P., Levelt, P. F., Fioletov, V. E., Dickerson, R. R., He, H., Lu, Z., and Streets, D. G.: Aura OMI observations of regional $SO_2$ and $NO_2$ pollution changes from 2005 to 2015, Atmospheric Chemistry and Physics, 16, 4605–4629, https://doi.org/10.5194/acp-16-4605-2016, 2016.

Kuenen, J. and Dore, C.: EMEP/EEA air pollutant emission inventory guidebook 2019: Uncertainties, Tech. rep., https://www.eea.europa.eu/publications/emep-eea-guidebook-2019/part-a-general-guidance-chapters/5-uncertainties, 2019.

Kuenen, J. J. P., Visschedijk, A. J. H., Jozwicka, M., and Denier van der Gon, H. A. C.: TNO-MACC-II emission inventory: a multi-year (2003-2009) consistent high-resolution European emission inventory for air quality modelling, Atmospheric Chemistry and Physics, 14, 10 963–10 976, https://doi.org/10.5194/acp-14-10963-2014, 2014.

Kurtenbach, R., Becker, K., Gomes, J., Kleffmann, J., Lörzer, J., Spittler, M., Wiesen, P., Ackermann, R., Geyer, A., and Platt, U.: Investigations of emissions and heterogeneous formation of HONO in a road traffic tunnel, Atmospheric Environment, 35, 3385–3394, https://doi.org/https://doi.org/10.1016/S1352-2310(01)00138-8, 2001.

Lambert, J.-C., Compernolle, S., Eichmann, K.-U., de Graaf, M., Hubert, D., Keppens, A., Kleipool, Q., Langerock, B., Sha, M., Verhoelst, T., Wagner, T., Ahn, C., Argyrouli, A., Balis, D., Chan, K., Smedt, I. D., Eskes, H., Fjæraa, A., Garane, K., Gleason, J., Goutail, F., Granville, J., Hedelt, P., Heue, K.-P., Jaross, G., Koukouli, M., Landgraf, J., Lutz, R., Nanda, S., Niemeijer, S., Pazmiño, A., Pinardi, G., Pommereau, J.-P., Richter, A., Rozemeijer, N., Sneep, M., Zweers, D. S., Theys, N., Tilstra, G., Torres, O., Valks, P., van Geffen, J., Vigouroux, C., Wang, P., and Weber, M.: Quarterly Validation Report of the Copernicus Sentinel-5 Precursor Operational Data Products #10: April 2018 – March 2021., Tech. rep., https://mpc-vdaf.tropomi.eu/ProjectDir/reports//pdf/S5P-MPC-IASB-ROCVR-10.01.00-20210326-signed.pdf, 2021.

Lambert, J.-C., Keppens, A., Compernolle, S., Eichmann, K.-U., de Graaf, M., Hubert, D., Langerock, B., Ludewig, A., Sha, M., Verhoelst, T., Wagner, T., Ahn, C., Argyrouli, A., Balis, D., Chan, K., Coldewey-Egbers, M., Smedt, I. D., Eskes, H., Fjæraa, A., Garane, K., Gleason, J., Goutail, F., Granville, J., Hedelt, P., Ahn, C., Heue, K.-P., Jaross, G., Kleipool, Q., Koukouli, M., Lutz, R., Velarte, M. M., Michailidis, K., Nanda, S., Niemeijer, S., Pazmiño, A., Pinardi, G., Richter, A., Rozemeijer, N., Sneep, M., Zweers, D. S., Theys, N., Tilstra, G., Torres, O., Valks, P., van Geffen, J., Vigouroux, C., Wang, P., and Weber., M.: Quarterly Validation Report of the Copernicus Sentinel-5 Precursor Operational Data Products #21: April 2018 – November 2023, Tech. rep., CAMS Cluster Service, https://doi.org/S5P-MPC-IASB-ROCVR-21.01.00-20231218, 2023.

Lamsal, L. N., Martin, R. V., Padmanabhan, A., van Donkelaar, A., Zhang, Q., Sioris, C. E., Chance, K., Kurosu, T. P., and Newchurch, M. J.: Application of satellite observations for timely updates to global anthropogenic NOx emission inventories, Geophysical Research Letters, 38, https://doi.org/https://doi.org/10.1029/2010GL046476, 2011.

Lamsal, L. N., Duncan, B. N., Yoshida, Y., Krotkov, N. A., Pickering, K. E., Streets, D. G., and Lu, Z.: U.S. NO2 trends (2005–2013): EPA Air Quality System (AQS) data versus improved observations from the Ozone Monitoring Instrument (OMI), Atmospheric Environment, 110, 130–143, https://doi.org/https://doi.org/10.1016/j.atmosenv.2015.03.055, 2015.

Lattuati, M.: Impact des emissions Europeennes sur le bilan de l'ozone tropospherique a l'interface de l'Europe et de l'Atlantique Nord: apport de la modelisation Lagrangienne et des mesures en altitude, Ph.D. thesis, Paris 6, 1997.

Levelt, P., van den Oord, G., Dobber, M., Malkki, A., Visser, H., de Vries, J., Stammes, P., Lundell, J., and Saari, H.: The ozone monitoring instrument, IEEE Transactions on Geoscience and Remote Sensing, 44, 1093–1101, https://doi.org/10.1109/TGRS.2006.872333, 2006.

Levelt, P. F., Joiner, J., Tamminen, J., Veefkind, J. P., Bhartia, P. K., Stein Zweers, D. C., Duncan, B. N., Streets, D. G., Eskes, H., van der A, R., McLinden, C., Fioletov, V., Carn, S., de Laat, J., DeLand, M., Marchenko, S., McPeters, R., Ziemke, J., Fu, D., Liu, X., Pickering,

K., Apituley, A., González Abad, G., Arola, A., Boersma, F., Chan Miller, C., Chance, K., de Graaf, M., Hakkarainen, J., Hassinen, S., Ialongo, I., Kleipool, Q., Krotkov, N., Li, C., Lamsal, L., Newman, P., Nowlan, C., Suleiman, R., Tilstra, L. G., Torres, O., Wang, H., and Wargan, K.: The Ozone Monitoring Instrument: overview of 14 years in space, Atmospheric Chemistry and Physics, 18, 5699–5745, https://doi.org/10.5194/acp-18-5699-2018, 2018.

Li, H., Zheng, B., Ciais, P., Boersma, K. F., Riess, T. C. V. W., Martin, R. V., Broquet, G., van der A, R., Li, H., Hong, C., Lei, Y., Kong, Y., Zhang, Q., and He, K.: Satellite reveals a steep decline in China’s CO<sub>2</sub> emissions in early 2022, Science Advances, 9, eadg7429, https://doi.org/10.1126/sciadv.adg7429, 2023.

Li, J. and Wang, Y.: Inferring the anthropogenic $NO_x$ emission trend over the United States during 2003–2017 from satellite observations: was there a flattening of the emission trend after the Great Recession?, Atmospheric Chemistry and Physics, 19, 15 339–15 352, https://doi.org/10.5194/acp-19-15339-2019, 2019.

Lin, J.-T.: Satellite constraint for emissions of nitrogen oxides from anthropogenic, lightning and soil sources over East China on a high-resolution grid, Atmospheric Chemistry and Physics, 12, 2881–2898, https://doi.org/10.5194/acp-12-2881-2012, 2012.

Lorente, A., Folkert Boersma, K., Yu, H., Dörner, S., Hilboll, A., Richter, A., Liu, M., Lamsal, L. N., Barkley, M., De Smedt, I., Van Roozendael, M., Wang, Y., Wagner, T., Beirle, S., Lin, J.-T., Krotkov, N., Stammes, P., Wang, P., Eskes, H. J., and Krol, M.: Structural uncertainty in air mass factor calculation for $NO_2$ and HCHO satellite retrievals, Atmospheric Measurement Techniques, 10, 759–782, https://doi.org/10.5194/amt-10-759-2017, 2017.

Mailler, S., Menut, L., Khvorostyanov, D., Valari, M., Couvidat, F., Siour, G., Turquety, S., Briant, R., Tuccella, P., Bessagnet, B., Colette, A., Létinois, L., Markakis, K., and Meleux, F.: CHIMERE-2017: from urban to hemispheric chemistry-transport modeling, Geoscientific Model Development, 10, 2397–2423, https://doi.org/10.5194/gmd-10-2397-2017, 2017.

Martin, R. V., Jacob, D. J., Chance, K., Kurosu, T. P., Palmer, P. I., and Evans, M. J.: Global inventory of nitrogen oxide emissions constrained by space-based observations of NO2 columns, Journal of Geophysical Research: Atmospheres, 108, https://doi.org/https://doi.org/10.1029/2003JD003453, 2003.

McGrath, M. J., Petrescu, A. M. R., Peylin, P., Andrew, R. M., Matthews, B., Dentener, F., Balkovič, J., Bastrikov, V., Becker, M., Broquet, G., Ciais, P., Fortems, A., Ganzenmüller, R., Grassi, G., Harris, I., Jones, M., Knauer, J., Kuhnert, M., Monteil, G., Munassar, S., Palmer, P. I., Peters, G. P., Qiu, C., Schelhaas, M.-J., Tarasova, O., Vizzarri, M., Winkler, K., Balsamo, G., Berchet, A., Briggs, P., Brockmann, P., Chevallier, F., Conchedda, G., Crippa, M., Dellaert, S., Denier van der Gon, H. A. C., Filipek, S., Friedlingstein, P., Fuchs, R., Gauss, M., Gerbig, C., Guizzardi, D., Günther, D., Houghton, R. A., Janssens-Maenhout, G., Lauerwald, R., Lerink, B., Luijkx, I. T., Moulas, G., Muntean, M., Nabuurs, G.-J., Paquirissamy, A., Perugini, L., Peters, W., Pilli, R., Pongratz, J., Regnier, P., Scholze, M., Serengil, Y., Smith, P., Solazzo, E., Thompson, R. L., Tubiello, F. N., Vesala, T., and Walther, S.: The consolidated European synthesis of $CO_2$ emissions and removals for EU27 and UK: 1990–2020, Earth System Science Data Discussions, 2023, 1–123, https://doi.org/10.5194/essd-2022-412, 2023.

Menut, L., Bessagnet, B., Khvorostyanov, D., Beekmann, M., Blond, N., Colette, A., Coll, I., Curci, G., Foret, G., Hodzic, A., Mailler, S., Meleux, F., Monge, J.-L., Pison, I., Siour, G., Turquety, S., Valari, M., Vautard, R., and Vivanco, M. G.: CHIMERE 2013: a model for regional atmospheric composition modelling, Geoscientific Model Development, 6, 981–1028, https://doi.org/10.5194/gmd-6-981-2013, 2013.

Menut, L., Bessagnet, B., Mailler, S., Pennel, R., and Siour, G.: Impact of Lightning NOx Emissions on Atmospheric Composition and Meteorology in Africa and Europe, Atmosphere, 11, https://doi.org/10.3390/atmos11101128, 2020.

Mijling, B. and van der A, R. J.: Using daily satellite observations to estimate emissions of short-lived air pollutants on a mesoscopic scale, Journal of Geophysical Research: Atmospheres, 117, https://doi.org/10.1029/2012jd017817, 2012.

Mijling, B., van der A, R. J., and Zhang, Q.: Regional nitrogen oxides emission trends in East Asia observed from space, Atmospheric Chemistry and Physics, 13, 12 003–12 012, https://doi.org/10.5194/acp-13-12003-2013, 2013.

Miyazaki, K., Eskes, H., Sudo, K., Boersma, K. F., Bowman, K., and Kanaya, Y.: Decadal changes in global surface $NO_x$ emissions from multi-constituent satellite data assimilation, Atmospheric Chemistry and Physics, 17, 807–837, https://doi.org/10.5194/acp-17-807-2017, 2017.

Munro, R., Lang, R., Klaes, D., Poli, G., Retscher, C., Lindstrot, R., Huckle, R., Lacan, A., Grzegorski, M., Holdak, A., Kokhanovsky, A., Livschitz, J., and Eisinger, M.: The GOME-2 instrument on the Metop series of satellites: instrument design, calibration, and level 1 data processing

– an overview, Atmospheric Measurement Techniques, 9, 1279–1301, https://doi.org/10.5194/amt-9-1279-2016, 2016.

OJE: DIRECTIVE (EU) 2016/2284 OF THE EUROPEAN PARLIAMENT AND OF THE COUNCIL of 14 December 2016 on the reduction of national emissions of certain atmospheric pollutants, amending Directive 2003/35/EC and repealing Directive 2001/81/EC, Official Journal of the European Union, Tech. rep., https://doi.org/S5P-MPC-IASB-ROCVR-21.01.00-20231218, 2016.

Owens, R. G. and Hewson, T.: ECMWF Forecast User Guide, Tech. rep., https://doi.org/https://doi.org/10.21957/m1cs7h, 2018.

Plauchu, R., Fortems-Cheiney, A., Broquet, G., Pison, I., Berchet, A., Potier, E., Dufour, G., Coman, A., Savas, D., Siour, G., and Eskes, H.: $NO_x$ emissions in France in 2019–2021 as estimated by the high spatial resolution assimilation of TROPOMI $NO_2$ observations, EGUsphere, 2024, 1–34, https://doi.org/10.5194/egusphere-2024-103, 2024.

Qu, Z., Henze, D. K., Capps, S. L., Wang, Y., Xu, X., Wang, J., and Keller, M.: Monthly top-down NOx emissions for China (2005–2012): A hybrid inversion method and trend analysis, Journal of Geophysical Research: Atmospheres, 122, 4600–4625, https://doi.org/https://doi.org/10.1002/2016JD025852, 2017.

Qu, Z., Henze, D. K., Cooper, O. R., and Neu, J. L.: Impacts of global $\mathrm{NO}_x$ inversions on $\mathrm{NO}_2$ and ozone simulations, Atmospheric Chemistry and Physics, 20, 13 109–13 130, https://doi.org/10.5194/acp-20-13109-2020, 2020.

Rijsdijk, P., Eskes, H., Dingemans, A., Boersma, F., Sekiya, T., Miyazaki, K., and Houweling, S.: Quantifying uncertainties of satellite $NO_2$ superobservations for data assimilation and model evaluation, EGUsphere, 2024, 1–42, https://doi.org/10.5194/egusphere-2024-632, 2024.

Savas, D., Dufour, G., Coman, A., Siour, G., Fortems-Cheiney, A., Broquet, G., Pison, I., Berchet, A., and Bessagnet, B.: Anthropogenic NOx Emission Estimations over East China for 2015 and 2019 Using OMI Satellite Observations and the New Inverse Modeling System CIF-CHIMERE, Atmosphere, 14, https://doi.org/10.3390/atmos14010154, 2023.

Schenkeveld, V. M. E., Jaross, G., Marchenko, S., Haffner, D., Kleipool, Q. L., Rozemeijer, N. C., Veefkind, J. P., and Levelt, P. F.: In-flight performance of the Ozone Monitoring Instrument, Atmospheric Measurement Techniques, 10, 1957–1986, https://doi.org/10.5194/amt-10-1957-2017, 2017.

Schindlbacher, S., Bradly, M., and Bernhard, U.: Uncertainties and recalculations of emission inventories submitted under CLRTAP, Tech. rep., CEIP, https://www.ceip.at/fileadmin/inhalte/ceip/00_pdf_other/2021/uncertainties_and_recalculations_of_emission_inventories_submitted_under_clrtap.pdf, 2021.

Schneider, P., Lahoz, W. A., and van der A, R.: Recent satellite-based trends of tropospheric nitrogen dioxide over large urban agglomerations worldwide, Atmospheric Chemistry and Physics, 15, 1205–1220, https://doi.org/10.5194/acp-15-1205-2015, 2015.

Sekiya, T., Miyazaki, K., Eskes, H., Sudo, K., Takigawa, M., and Kanaya, Y.: A comparison of the impact of TROPOMI and OMI tropospheric $NO_2$ on global chemical data assimilation, Atmospheric Measurement Techniques, 15, 1703–1728, https://doi.org/10.5194/amt-15-1703-2022, 2022.

Silvern, R. F., Jacob, D. J., Mickley, L. J., Sulprizio, M. P., Travis, K. R., Marais, E. A., Cohen, R. C., Laughner, J. L., Choi, S., Joiner, J., and Lamsal, L. N.: Using satellite observations of tropospheric $NO_2$ columns to infer long-term trends in US $NO_x$ emissions: the importance of accounting for the free tropospheric $NO_2$ background, Atmospheric Chemistry and Physics, 19, 8863–8878, https://doi.org/10.5194/acp-19-8863-2019, 2019.

Stavrakou, T., Müller, J.-F., Boersma, K. F., De Smedt, I., and van der A, R. J.: Assessing the distribution and growth rates of NOx emission sources by inverting a 10-year record of NO2 satellite columns, Geophysical Research Letters, 35, https://doi.org/https://doi.org/10.1029/2008GL033521, 2008.

Stavrakou, T., Müller, J.-F., Boersma, K. F., van der A, R. J., Kurokawa, J., Ohara, T., and Zhang, Q.: Key chemical $NO_x$ sink uncertainties and how they influence top-down emissions of nitrogen oxides, Atmospheric Chemistry and Physics, 13, 9057–9082, https://doi.org/10.5194/acp-13-9057-2013, 2013.

Super, I., Dellaert, S. N. C., Visschedijk, A. J. H., and Denier van der Gon, H. A. C.: Uncertainty analysis of a European high-resolution emission inventory of $CO_2$ and CO to support inverse modelling and network design, Atmospheric Chemistry and Physics, 20, 1795–1816, https://doi.org/10.5194/acp-20-1795-2020, 2020.

Szopa, S.and Foret, G. M. L. C. A.: Impact of large scale circulation on European summer surface ozone: consequences for modeling, Atmospheric Environment, 43, https://doi.org/doi:10.1016/j.atmosenv.2008.10.0390, 2008.

Tilstra, L. G., de Graaf, M., Trees, V. J. H., Litvinov, P., Dubovik, O., and Stammes, P.: A directional surface reflectance climatology determined from TROPOMI observations, Atmospheric Measurement Techniques, 17, 2235–2256, https://doi.org/10.5194/amt-17-2235-2024, 2024.

van der A, R. J., Eskes, H. J., Boersma, K. F., van Noije, T. P. C., Van Roozendael, M., De Smedt, I., Peters, D. H. M. U., and Meijer, E. W.: Trends, seasonal variability and dominant NOx source derived from a ten year record of NO2 measured from space, Journal of Geophysical Research: Atmospheres, 113, https://doi.org/https://doi.org/10.1029/2007JD009021, 2008.

van der A, R. J., Ding, J., and Eskes, H.: Monitoring European anthropogenic NOx emissions from space, EGUsphere, 2024, 1–20, https://doi.org/10.5194/egusphere-2023-3099, 2024.

van Geffen, J., Boersma, K. F., Eskes, H., Sneep, M., ter Linden, M., Zara, M., and Veefkind, J. P.: S5P TROPOMI $NO_2$ slant column retrieval: method, stability, uncertainties and comparisons with OMI, Atmospheric Measurement Techniques, 13, 1315–1335, https://doi.org/10.5194/amt-13-1315-2020, 2020.

van Geffen, J., Eskes, H., Compernolle, S., Pinardi, G., Verhoelst, T., Lambert, J.-C., Sneep, M., ter Linden, M., Ludewig, A., Boersma, K. F., and Veefkind, J. P.: Sentinel-5P TROPOMI $NO_2$ retrieval: impact of version v2.2 improvements and comparisons with OMI and ground-based data, Atmospheric Measurement Techniques, 15, 2037–2060, https://doi.org/10.5194/amt-15-2037-2022, 2022a.

van Geffen, J., Eskes, H., K.F., B., and Veefkind, J.: TROPOMI ATBD of the total and tropospheric NO2 data products, Tech. rep., https://sentinel.esa.int/documents/247904/2476257/sentinel-5p-tropomi-atbd-no2-data-products, 2022b.

Veefkind, J., Aben, I., McMullan, K., Förster, H., de Vries, J., Otter, G., Claas, J., Eskes, H., de Haan, J., Kleipool, Q., van Weele, M., Hasekamp, O., Hoogeveen, R., Landgraf, J., Snel, R., Tol, P., Ingmann, P., Voors, R., Kruizinga, B., Vink, R., Visser, H., and Levelt, P.: TROPOMI on the ESA Sentinel-5 Precursor: A GMES mission for global observations of the at-

mospheric composition for climate, air quality and ozone layer applications, Remote Sensing of Environment, 120, 70–83, https://doi.org/https://doi.org/10.1016/j.rse.2011.09.027, the Sentinel Missions - New Opportunities for Science, 2012.

Veefkind, J. P., de Haan, J. F., Sneep, M., and Levelt, P. F.: Improvements to the OMI $O_2$–$O_2$ operational cloud algorithm and comparisons with ground-based radar–lidar observations, Atmospheric Measurement Techniques, 9, 6035–6049, https://doi.org/10.5194/amt-9-6035-2016, 2016.

Verhoelst, T., Compernolle, S., Pinardi, G., Lambert, J.-C., Eskes, H. J., Eichmann, K.-U., Fjæraa, A. M., Granville, J., Niemeijer, S., Cede, A., Tiefengraber, M., Hendrick, F., Pazmiño, A., Bais, A., Bazureau, A., Boersma, K. F., Bognar, K., Dehn, A., Donner, S., Elokhov, A., Gebetsberger, M., Goutail, F., Grutter de la Mora, M., Gruzdev, A., Gratsea, M., Hansen, G. H., Irie, H., Jepsen, N., Kanaya, Y., Karagkiozidis, D., Kivi, R., Kreher, K., Levelt, P. F., Liu, C., Müller, M., Navarro Comas, M., Piters, A. J. M., Pommereau, J.-P., Portafaix, T., Prados-Roman, C., Puentedura, O., Querel, R., Remmers, J., Richter, A., Rimmer, J., Rivera Cárdenas, C., Saavedra de Miguel, L., Sinyakov, V. P., Stremme, W., Strong, K., Van Roozendael, M., Veefkind, J. P., Wagner, T., Wittrock, F., Yela González, M., and Zehner, C.: Ground-based validation of the Copernicus Sentinel-5P TROPOMI $NO_2$ measurements with the NDACC ZSL-DOAS, MAX-DOAS and Pandonia global networks, Atmospheric Measurement Techniques, 14, 481–510, https://doi.org/10.5194/amt-14-481-2021, 2021.

Vestreng, V., Breivik, K.and Adams, M., Wagner, A., Goodwin, J., Rozovskaya, O., and Oacyna, J.: Inventory Review 2005 - Emission Data reported to CLRTAP and under the NEC Direc-tive - Initial review for HMs and POPs, Tech. rep., 2005.

Visser, A. J., Boersma, K. F., Ganzeveld, L. N., and Krol, M. C.: European $\mathrm{NO}_x$ emissions in WRF-Chem derived from OMI: impacts on summertime surface ozone, Atmospheric Chemistry and Physics, 19, 11 821–11 841, https://doi.org/10.5194/acp-19-11821-2019, 2019.

Zheng, B., Geng, G., Ciais, P., Davis, S. J., Martin, R. V., Meng, J., Wu, N., Chevallier, F., Broquet, G., Boersma, F., van der A, R., Lin, J., Guan, D., Lei, Y., He, K., and Zhang, Q.: Satellite-based estimates of decline and rebound in China’s CO<sub>2</sub> emissions during COVID-19 pandemic, Science Advances, 6, eabd4998, https://doi.org/10.1126/sciadv.abd4998, 2020.

Zheng, F., Yu, T., Cheng, T., Gu, X., and Guo, H.: Intercomparison of tropospheric nitrogen dioxide retrieved from Ozone Monitoring Instrument over China, Atmospheric Pollution Research, 5, 686–695, https://doi.org/https://doi.org/10.5094/APR.2014.078, 2014.